U.PORTO

FEUP FACULDADE DE ENGENHARIA
UNIVERSIDADE DO PORTO

FFT-based Homogenization Methods

Professor:
Francisco Manuel Andrade Pires

Student:
José Luís Passos Vila-Chã

Report presented under the scope of the
Doctoral Program in Mechanical Engineering

Porto, September 2021

Page intentionally left blank.

Contents

List of Figures

List of Tables

Page intentionally left blank.

Chapter 1

Continuum Mechanics and Finite Element Method

This chapter deals with the concepts needed to described the behavior of a solid undergoing large deformation, as well as, the conservation principles that ensure its mechanical equilibrium. It also presents a succint overview of the Finite Element Method as a tool to solve mechanical initial value equilibrium problem. These topics are broadly covered in the literature and here the approach used follows **?**,

1.1 Kinematics of Deformation

1.1.1 Motion

Let a deformable body $\mathscr{B}$ occupy an open region Ω_0 of the tridimensional Euclidean space $\mathscr{E}$ with a regular boundary $\partial\Omega_0$ in its reference configuration. Its motion, depicted in Figure **??**, is defined by a smooth one-to-one function

$$\boldsymbol{\varphi}\colon \Omega \times \mathscr{R} \to \mathscr{E}, \tag{1.1}$$

mapping each material particle of coordinates $\boldsymbol{X}$ in the reference configuration to its position $\boldsymbol{x}$ in the deformed configuration, for a given instant of time t, as

$$\boldsymbol{x} = \boldsymbol{\varphi}(\boldsymbol{X}, t). \tag{1.2}$$

Thus, the displacement field is defined as

$$\boldsymbol{u}(\boldsymbol{X}, t) = \boldsymbol{\varphi}(\boldsymbol{X}, t) - \boldsymbol{X}, \tag{1.3}$$

and, since the function that defines the motion is one-to-one, the reference configuration can be recovered as

$$\boldsymbol{X} = \boldsymbol{\varphi}^{-1}(\boldsymbol{x}, t) = \boldsymbol{x} - \boldsymbol{u}(\boldsymbol{\varphi}^{-1}(\boldsymbol{x}, t), t), \tag{1.4}$$

where $\boldsymbol{\varphi}^{-1}$ is the reference mapping function.

1.1.2 Material and spatial descriptions

Dealing with finite deformations, the behavior of the body under analysis can be described with respect to the reference configuration, using the so-called material or Lagrangian description, or to the deformed configuration, using the so-called spatial or Eulerian description.

In the Lagrangian description any field, be it scalar, vectorial or tensorial defined over the body is expressed as a function of the reference configuration, $\boldsymbol{X} \in \Omega_0$. On the other hand, the Eulerian descritpion of same field is done using the deformed configuration, $\boldsymbol{x} \in \Omega$.

As such let $\alpha(\boldsymbol{x}, t)$ be a spatial field and $\beta(\boldsymbol{X}, t)$ a material field. Their material α_m and spatial β_s desctiptions are given by

$$\alpha_m(\boldsymbol{X}, t) = \alpha(\boldsymbol{\varphi}(\boldsymbol{X}, t), t), \tag{1.5}$$

$$\beta_s(\boldsymbol{x}, t) = \beta(\boldsymbol{\varphi}^{-1}(\boldsymbol{x}, t), t), \tag{1.6}$$

noting that any field associated with a motion of $\mathscr{B}$ can be expressed as a function of time and material or spatial position.

The same distinction between material and spatial descriptions applies to operators such as the divergence and the gradient. The spatial and material gradients, ∇ and ∇_0, respectively, are defined as

$$\nabla\alpha = \frac{\partial}{\partial \boldsymbol{x}}\alpha(\boldsymbol{x}, t), \quad \nabla_0\beta = \frac{\partial}{\partial \boldsymbol{X}}\beta(\boldsymbol{X}, t), \tag{1.7}$$

where the derivatives are taken with respect to the spatial and reference configuration accordingly.

1.1.3 Deformation gradient

The deformation gradient, a second order tensor denoted by $\boldsymbol{F}$, is defined as

$$\boldsymbol{F}(\boldsymbol{X}, t) \equiv \nabla_0\boldsymbol{\varphi}(\boldsymbol{X}, t) = \frac{\partial \boldsymbol{x}}{\partial \boldsymbol{X}}, \tag{1.8}$$

or, taking into account that

$$\boldsymbol{x} = \boldsymbol{X} + \boldsymbol{u}(\boldsymbol{X}, t), \tag{1.9}$$

it can be expressed as

$$\boldsymbol{F}(\boldsymbol{X}, t) = \boldsymbol{I} + \nabla_0 u. \tag{1.10}$$

The deformation gradient relates the relative position between two neighboring material particles before and after deformation. To see this let $\boldsymbol{X}$ be the coordinates of some material prickle in the reference configuration and $\boldsymbol{X} + d\boldsymbol{X}$ the coordinates of some material particle in its neighborhood, their corresponding coordinates in the deformed configuration are given by

$$\boldsymbol{X} = \boldsymbol{x} + \boldsymbol{u}(\boldsymbol{X}, t), \tag{1.11}$$

$$\boldsymbol{X} + d\boldsymbol{X} = \boldsymbol{x} + d\boldsymbol{x} + \boldsymbol{u}(\boldsymbol{X} + d\boldsymbol{X}, t). \tag{1.12}$$

Subtracting Equation (1.11) to Equation (1.12), it is found that

$$d\boldsymbol{X} = d\boldsymbol{x} + \boldsymbol{u}(\boldsymbol{X} + d\boldsymbol{X}, t) - \boldsymbol{u}(\boldsymbol{X}, t) \tag{1.13}$$
$$= (\boldsymbol{I} + \nabla_0 \boldsymbol{u}(\boldsymbol{X}, t))\, d\boldsymbol{x} \tag{1.14}$$
$$= \boldsymbol{F}\, d\boldsymbol{x}. \tag{1.15}$$

Due to this relation, it can be shown that the determinat of the deformation gradient has a physical meaning. It is the local unit volume change, that is,

$$J \equiv \det \boldsymbol{F} = \frac{dv}{dv_0}, \tag{1.16}$$

where dv_0 is an infinitesimal volume of the body in its reference configuration and dv the infinitesimal volume after deformation.

Isochoric/Volumetric decomposition

Any deformation can be locally decomposed in volumetric and isochoric (or distortional) components. From Equation (1.16) it can be gathered that an isochoric deformation is characterized by $J = 1$. As such, the deformation gradient can be decomposed as

$$\boldsymbol{F} = \boldsymbol{F}_{\text{iso}} \boldsymbol{F}_{\text{vol}} = \boldsymbol{F}_{\text{vol}} \boldsymbol{F}_{\text{iso}}, \tag{1.17}$$

where the isochoric and columetric components are defined by

$$\boldsymbol{F}_{\text{iso}} = (\det \boldsymbol{F})^{-\frac{1}{3}}, \quad \boldsymbol{F}_{\text{vol}} = (\det \boldsymbol{F})^{\frac{1}{3}} \boldsymbol{I}. \tag{1.18}$$

Polar decomposition

The deformation gradient can also be decomposed in rotation and stretch components, the so-called polar decomposition, defined as

$$\boldsymbol{F} = \boldsymbol{R}\boldsymbol{U} = \boldsymbol{V}\boldsymbol{R}, \tag{1.19}$$

where $\boldsymbol{R}$ is the proper orthogonal rotation tensor and $\boldsymbol{U}$ and $\boldsymbol{V}$ are the symmetric positive right and left stretch tensors, respectively.

Equation (1.19) has a physical interpretation with the right polar decomposition ($\boldsymbol{F} = \boldsymbol{R}\boldsymbol{U}$) corresponding to a stretch mapping followed by a rotation, and the left polar decomposition ($\boldsymbol{F} = \boldsymbol{V}\boldsymbol{R}$) corresponding to a rotation followed by a stretch mapping. The right $\boldsymbol{U}$ and left $\boldsymbol{V}$ stretch tensors are related through the rotation matrix $\boldsymbol{R}$ as

$$\boldsymbol{V} = \boldsymbol{R}\boldsymbol{U}\boldsymbol{R}^T, \tag{1.20}$$

and can be obtained from deformation gradient by

$$\boldsymbol{C} \equiv \boldsymbol{U}^2 = \boldsymbol{F}^T\boldsymbol{F}, \quad \boldsymbol{B} \equiv \boldsymbol{V}^2 = \boldsymbol{F}\boldsymbol{F}^T., \tag{1.21}$$

where $\boldsymbol{C}$ and $\boldsymbol{B}$ are the right and left Cauchy-Green strain tensors.

Since $\boldsymbol{U}$ and $\boldsymbol{V}$ are symmetric tensors, they admit the spectral decomposition

$$\boldsymbol{U} = \sum_{i=1}^{3} \lambda_i \boldsymbol{E}_i^* \otimes \boldsymbol{E}_i^*, \quad \boldsymbol{V} = \sum_{i=1}^{3} \lambda_i \boldsymbol{e}_i^* \otimes \boldsymbol{e}_i^*, \tag{1.22}$$

where λ_i, $i = 1,2,3$, are the eigenvalues of both $\boldsymbol{U}$ and $\boldsymbol{V}$ and $\boldsymbol{E}_i^*$ and $\boldsymbol{e}_i^*$ are the respective eigenvectors.

The eigenvectors of left $\boldsymbol{V}$ and right $\boldsymbol{U}$ stretch tensors are related through

$$\boldsymbol{e}_i^* = \boldsymbol{R}\boldsymbol{E}_i^*. \tag{1.23}$$

forming two orthogonal bases. These vectors define the Lagrangian and Eulerian principal directions, respectively, allowing for the expression of the local stretching from a material particle, associated with any deformation, as a superposition of stretches along the three mutual orthogonal directions.,

For solid dynamical problems, material time differentiation of the deformation and the strain measures need to be introduced. The first and second derivative of the displacement field $u(X,t)$. li.e. the material velocity and acceleration, $\dot{u}$ and $\ddot{u}$, respectively, result in) where (2.2) can be used to show that due to the constant initial position X)

$$\hat{\boldsymbol{x}}(\boldsymbol{X},t) \equiv \overline{\boldsymbol{u}}(\boldsymbol{X},t)$$

According to (2.3), the material velocity gradient results in With the material gradient operator Grad$(\cdot)$. Equation (2.23) can be reformulated, yielding the Ispatial velocity gradient and its symmetric part

$$\boldsymbol{L} = \dot{\boldsymbol{F}} \cdot \boldsymbol{F}^{-1}$$
$$\boldsymbol{D} = \tfrac{1}{2}\left(\boldsymbol{L} + \boldsymbol{L}^{\top}\right)$$

The rate of the Green-Lagrange strain tensor results in the material strain rate tensor

$$\dot{E}_{\mathrm{GL}} = \frac{1}{2}\dot{C} = \boldsymbol{F}^{\mathrm{T}} \cdot \boldsymbol{D} \cdot \boldsymbol{F}$$

which can be expressed as pull-back of the symmetric spatial strain rate tensor D. Via the Liederivative or Oldroyd-Lie derivative of the Euler-Almansi strain tensor $\mathscr{L}_t\left[\boldsymbol{E}_{\mathrm{EA}}\right]$, which represents an objective material time derivative, a relation to the rate of the Euler-Almansi strain tensor is achieved as

$$\mathscr{L}_t\left[\boldsymbol{E}_{\mathrm{EA}}\right] = \varphi\left[\frac{\mathrm{d}}{\mathrm{d}t}\left(\varphi^{-1}\left[\boldsymbol{E}_{\mathrm{EA}}\right]\right)\right] = \boldsymbol{D} = \boldsymbol{F}^{-\top} \cdot \dot{\boldsymbol{E}}_{\mathrm{GL}} \cdot \boldsymbol{F}^{-1}$$

Moreover, the rate of volume changes is described by $\dot{J}$ and can be expressed through

$$\dot{J} = J \operatorname{tr} \boldsymbol{D}$$

1.2 Strain tensors

In Continuum Mechanics there are two main families of strain tensors derived from the deformation gradient and used to describe the body deformation. The Lagrange

family strain tensors are defined as

$$\boldsymbol{E}^{(m)} = \begin{cases} \dfrac{1}{m}(\boldsymbol{U}^m - \boldsymbol{I}), & m \neq 0, \\ \ln(\boldsymbol{U}), & m = 0, \end{cases} \tag{1.24}$$

where m is a real number, and likewise, the Euler family strain tensors are defined as

$$\boldsymbol{\varepsilon}^{(m)} = \begin{cases} \dfrac{1}{m}(\boldsymbol{V}^m - \boldsymbol{I}), & m \neq 0, \\ \ln(\boldsymbol{V}), & m = 0, \end{cases} \tag{1.25}$$

where m is also real number.

In particular, choosing $m = 0$, one obtains the so-called material and spatial logarithmic strain tensors

$$\boldsymbol{E}^{(0)} \equiv \ln[\boldsymbol{U}] = \sum_{i=1}^{3} \ln \lambda_i \boldsymbol{E}_i^* \otimes \boldsymbol{E}_i^*, \tag{1.26}$$

$$\boldsymbol{e}^{(0)} \equiv \ln[\boldsymbol{V}] = \sum_{i=1}^{3} \ln \lambda_i \boldsymbol{e}_i^* \otimes \boldsymbol{e}_i^*. \tag{1.27}$$

1.3 Forces and stress measures

The deformation of a body is intrinsically related to the forces acting on it. These forces can be divided in two classes, from a purely mechanical point of view: volume (or body) forces, proportional to the mass contained in a volume element, as such measured in force per unit volume, and surface forces, acting on the surface of a volume element, measured as force per unit area. Related to the latter is the concept of stress, that can be described mathematically by second order tensors with different definitions.

Cauchy stress tensor

According to Cauchy's theorem the relation between the so-called Cauchy stress vector, $\boldsymbol{t}(\boldsymbol{x}, \boldsymbol{n})$, and the unitary outward vector normal to the deformed surface under analysis, $\boldsymbol{n}$, is linear and given by

$$\boldsymbol{t}(\boldsymbol{x}, \boldsymbol{n}) \equiv \boldsymbol{\sigma}(\boldsymbol{x})\boldsymbol{n}, \tag{1.28}$$

where $\boldsymbol{\sigma}$ is the second order Cauchy stress tensor.

The Cauchy stress vector is naturally associated with the deformed configured and thus, expressed in a spatial description and measured in force per unit deformed area. It must also be noted that as a consequence of the balance of angular momentum, the Cauchy stress tensor is symmetric.

First Piola-Kirchhoff stress tensor

The First Piola-Kirchhoff stress tensor, $\boldsymbol{P}$, can be regarded as the material counterpart of the Cauchy stress tensor, as it establishes a linear dependence between the stress

vector $\boldsymbol{t}_0(\boldsymbol{X},\boldsymbol{m})$, measured in force per unit reference area, and the unitary outward vector normal to the undeformed surface under analysis, $\boldsymbol{m}$,

$$\boldsymbol{t}_0 = \boldsymbol{P}\boldsymbol{m}, \tag{1.29}$$

which must related to the Cauchy stress vector by

$$\boldsymbol{t}_0 = \frac{\mathrm{d}a}{\mathrm{d}a_0}\boldsymbol{t} = \frac{\mathrm{d}a}{\mathrm{d}a_0}\boldsymbol{\sigma}\boldsymbol{n}, \tag{1.30}$$

where $\mathrm{d}a$ is the infinitesimal deformed area normal to the unitary vector $\boldsymbol{n}$ and $\mathrm{d}a_0$ the corresponding undeformed are normal to $\boldsymbol{m}$. It can be shown that the relation between da and da_0 is

$$\frac{da}{da_0}\boldsymbol{n} = J\boldsymbol{F}^{-T}\boldsymbol{m}, \tag{1.31}$$

and substituting on the equation above motivates the following definition

$$\boldsymbol{P} \equiv J\boldsymbol{\sigma}\boldsymbol{F}^{-T}, \tag{1.32}$$

where J is the determinant of the deformation gradient $\boldsymbol{F}$ and $\boldsymbol{\sigma}$ is the Cauchy stress tensor. From Equation (1.32), one gathers that, in general, the First Piola-Kirchhoff stress tensor is not symmetric.

Kirchhoff stress tensor

The Kirchhoff stress tensor, $\boldsymbol{\tau}$, is a widely used symmetric tensor, defined as

$$\boldsymbol{\tau} \equiv J\boldsymbol{\sigma}. \tag{1.33}$$

Deviatoric/Hydrostatic decomposition

The Cauchy stress tensor, $\boldsymbol{\sigma}$, can split as

$$\boldsymbol{\sigma} = \boldsymbol{\sigma}_d - p\boldsymbol{I}, \tag{1.34}$$

where p is the hydrostatic pressure defined as

$$p \equiv -\frac{1}{3}\mathrm{tr}\,[\boldsymbol{\sigma}], \tag{1.35}$$

and $\boldsymbol{\sigma}_d$ is the deviatoric stress defined as

$$\sigma_d \equiv \boldsymbol{\sigma} - p\boldsymbol{I}. \tag{1.36}$$

1.4 Fundamental conservation principles

In Continuum Mechanics. there is a set of conservation principles and thermodynamic laws, that irrespective of the quantities used to describe the mechanical behavior of a body undergoing large deformations must always be satisfied.

Principle of mass conservation

The principle of mass conservation can be stated as

$$\dot{\rho} + \rho \operatorname{div} \dot{\boldsymbol{u}}(\boldsymbol{x}) = 0, \tag{1.37}$$

where ρ is the material density measured in mass per unit deformed volume.

Principle of linear momentum conservation

The principle of linear momentum conservation can be stated in both material and spatial description. In a spatial description it reads

$$\begin{cases} \operatorname{div} \boldsymbol{\sigma}(\boldsymbol{x}) + \boldsymbol{b} = \rho \ddot{\boldsymbol{u}}(\boldsymbol{x}), & \forall \boldsymbol{x} \in \Omega, \\ \boldsymbol{t}(\boldsymbol{x}, \boldsymbol{n}) = \boldsymbol{\sigma}(\boldsymbol{x}) \boldsymbol{n}, & \forall \boldsymbol{x} \in \partial\Omega, \end{cases} \tag{1.38}$$

where $\boldsymbol{b}$ is the body forces field measured as per unit deformed volume.

One can also write the principle of linear momentum conservation in material coordinates, as

$$\begin{cases} \operatorname{div}_0 \boldsymbol{P}(\boldsymbol{X}) + \boldsymbol{b}_0 = \rho_0 \ddot{\boldsymbol{u}}(\boldsymbol{X}), & \forall \boldsymbol{x} \in \Omega_0, \\ \boldsymbol{t}_0(\boldsymbol{X}, \boldsymbol{m}) = \boldsymbol{P}(\boldsymbol{X}) \boldsymbol{m}, & \forall \boldsymbol{x} \in \partial\Omega_0, \end{cases} \tag{1.39}$$

where $\boldsymbol{b}_0$ is the body forces field, measured in force per unit undeformed volume, and ρ_0 is the material density, measured in mass per unit undeformed volume. Both these quantities can be found from their spatial counterparts as

$$\boldsymbol{b}_0 = J\, \boldsymbol{b}, \quad \rho_0 = J\, \rho. \tag{1.40}$$

Equations (1.38) and (1.39) are the so-called strong, point-wise or local equilibrium equations, as they enforce the mechanical equilibrium at every material particle of the body.

First principle of thermodynamics

$$\rho \dot{e} = \boldsymbol{\sigma} : \boldsymbol{D} + \rho r - \operatorname{div} \boldsymbol{q}, \tag{1.41}$$

where e is the specific internal energy field, r is the density of heat production field and $\boldsymbol{q}$ is the heat flux vector field. The second order tensor $\boldsymbol{D}$ denotes a strain rate measure, such that the double contraction $\boldsymbol{\sigma} : \boldsymbol{D}$ represents the stress power per unit volume in the deformed configuration of body. In material coordinates, it reads

$$\rho_0 \frac{\partial e}{\partial t} = \boldsymbol{P} : \frac{\partial \boldsymbol{F}}{\partial t} + \rho_0 r - \operatorname{div}_0 \boldsymbol{q}_0, \tag{1.42}$$

where $\boldsymbol{q}_0$ is the Piola transformation of $\boldsymbol{q}$, i.e.,

$$\boldsymbol{q}_0 = J \boldsymbol{F}^{-T} \boldsymbol{q}, \tag{1.43}$$

and all state variables depend on the material coordinates $\boldsymbol{X}$.

Second principle of thermodynamics

The local entropy balance can written as

$$\rho \dot{s} = -\operatorname{div}\left[\frac{\boldsymbol{q}}{\theta}\right] + \frac{\rho r}{\theta} + \hat{s}, \tag{1.44}$$

where $\hat{s}$ is the entropy production. The second principle of thermodynamics postulates that the changes in the entropy in the universe can never be negative, which is mathematically expressed by

$$\hat{s} \geq 0, \tag{1.45}$$

yielding

$$\rho \dot{s} + \operatorname{div}\left[\frac{\boldsymbol{q}}{\theta}\right] - \frac{\rho r}{\theta} \geq 0, \tag{1.46}$$

where θ and s are the temperature and specific entropy fields respectively. In a material description, it reads

$$\rho_0 \frac{\partial s}{\partial t} + \operatorname{div}_0\left[\frac{\boldsymbol{q}_0}{\theta}\right] - \frac{\rho_0 r}{\theta} \geq 0, \tag{1.47}$$

where all state variables depend on the material coordinates $\boldsymbol{X}$.

Clausius-Duhem inequality

Combining the first and second thermodynamic principles yields

$$\rho \dot{s} + \operatorname{div}\left[\frac{\boldsymbol{q}}{\theta}\right] - \frac{1}{\theta}(\rho \dot{e} - \boldsymbol{\sigma} : \boldsymbol{D} + \operatorname{div} \boldsymbol{q}) \geq 0, \tag{1.48}$$

From the definition of the specific Helmholtz free energy

$$\psi \equiv e - \theta s, \tag{1.49}$$

and defining the temperature field gradient as $\boldsymbol{g} = \nabla\theta$, it is possible to establish the so-called Clausius-Duhem inequality in the spatial description as

$$\underbrace{\boldsymbol{\sigma} : \boldsymbol{D} - \rho\left(\dot{\psi} + s\dot{\theta}\right)}_{\mathcal{D}_{\text{mech}}} \underbrace{- \frac{1}{\theta}\boldsymbol{q} \cdot \boldsymbol{g}}_{\mathcal{D}_{\text{cond}}} \geq 0, \tag{1.50}$$

where the identity

$$\operatorname{div}\left[\frac{\boldsymbol{q}}{\theta}\right] = \frac{1}{\theta}\operatorname{div} \boldsymbol{q} - \frac{1}{\theta^2}\boldsymbol{q} \cdot \nabla\theta. \tag{1.51}$$

is used.

From a physical point of view, the Clausius-Duhem inequality states that the energy dissipation per unit deformed volume is always non-negative. Moreover the terms in the inequalitiy can be splited between the mechanical internal dissipation $\mathcal{D}_{\text{mech}}$ and the dissipation due to heat conduction $\mathcal{D}_{\text{cond}}$. From

$$\hat{s} = \boldsymbol{\sigma} : \boldsymbol{D} - \rho\left(\dot{\psi} + s\dot{\theta}\right) - \frac{1}{\theta}\boldsymbol{q} \cdot \boldsymbol{g}, \tag{1.52}$$

assuming that the process leads to an uniform temperature distribution, yields for the mechanical dissipation $\mathcal{D}_{\text{mech}}$,

$$\mathcal{D}_{\text{mech}} = \hat{s}|_{\theta \text{ uniform}} = \boldsymbol{\sigma} : \boldsymbol{D} - \rho\left(\dot{\psi} + s\dot{\theta}\right), \tag{1.53}$$

since conduction is excluded and only mechanical and temperature transient effects remain. If on the other hand, only conduction effects are retained, i.e., assuming the process to be isothermic, isochoric and isovolumetric, the dissipation due to conduction, $\mathcal{D}_{\text{cond}}$, is obtained as

$$\mathcal{D}_{\text{cond}} = -\frac{1}{\theta}\boldsymbol{q}\cdot\boldsymbol{g}. \tag{1.54}$$

Equation (1.50) can also be written as

$$\boldsymbol{\tau} : \boldsymbol{D} - \rho_0\left(\dot{\psi} + s\dot{\theta}\right) - \frac{J}{\theta}\boldsymbol{q}\cdot\boldsymbol{g} \geq 0, \tag{1.55}$$

multiplying it by J and attending to the definition of the Kirchhoff stress tensor, where the left hand side represents now the energy dissipation per unit reference volume.

1.5 Mechanical constitutive initial value problem

In Continuum Mechanics, a constitutive model is a set of equations, also called constitutive equations, establishing the stress-strain relation for some material. Before going further, it is important to define a thermokinetic process of a body $\mathscr{B}$ as

$$\text{thermokinetic process:} \quad \{\boldsymbol{\varphi}(\boldsymbol{X},t), \theta(\boldsymbol{X},t)\}, \tag{1.56}$$

ans a calordynamic process of $\mathscr{B}$ as

$$\text{calorodynamic process:} \quad \{\boldsymbol{\sigma}(\boldsymbol{X},t), e(\boldsymbol{X},t), s(\boldsymbol{X},t), r(\boldsymbol{X},t), \boldsymbol{b}(\boldsymbol{X},t), \boldsymbol{q}(\boldsymbol{X},t)\}, \tag{1.57}$$

which satisfies the fundamental conservation principles previously introduced.

It is also important to note that any constitutive model must satisfy a set of constitutive axioms, explained in detail by **?**. As these are too general to be used directly in practice, a particular case of the general history functional-based constitutive theory based on the thermodynamics with internal variables approach is used.

1.5.1 Thermodynamics with internal variables

The values of $\boldsymbol{\sigma}$, ψ, s and $\boldsymbol{q}$ at a material particle define its thermodynamic state, assuming $\boldsymbol{b}$ follows from the balance of linear momentum and r from the energy balance equation. In thermodynamics with interval variables approach, that thermodynamic state is assumed to be completely defined by the instantaneous values of a finite number of state variables

$$\{\boldsymbol{F}, \theta, \boldsymbol{g}, \boldsymbol{\alpha}\}. \tag{1.58}$$

at a given instant of the calorodynamic process, where

$$\boldsymbol{\alpha} = \{\alpha_k\} \tag{1.59}$$

is a set of internal variables, scalar or tensorial in nature, associated with dissipative mechanisms. As such, the accuracy of the constitutive model depends strongly on the appropriate choice of internal variables, as these contain the relevant information about the thermodynamical history of the material.

Accordingly, the specific Helmholtz free energy is postulated to follow

$$\psi = \psi(\boldsymbol{F}, \theta, \boldsymbol{\alpha}). \tag{1.60}$$

To find the constitutive equations for the stress tensor and the entropy, one can substitute

$$\dot{\psi} = \frac{\partial \psi}{\partial \boldsymbol{F}} : \dot{\boldsymbol{F}} + \frac{\partial \psi}{\partial \theta}\dot{\theta} + \frac{\partial \psi}{\partial \alpha_k}\dot{\alpha}_k, \tag{1.61}$$

found from the chain rule, on the Clausius-Duhem equation, Equation (1.50), obtaining

$$\left(\boldsymbol{\sigma}\boldsymbol{F}^{-T} - \rho\frac{\partial \psi}{\partial \boldsymbol{F}}\right) : \dot{\boldsymbol{F}} - \rho\left(s + \frac{\partial \psi}{\partial \theta}\right)\dot{\theta} - \rho\frac{\partial \psi}{\partial \alpha_k}\dot{\alpha}_k - \frac{1}{\theta}\boldsymbol{q}\cdot\boldsymbol{g} \geq 0, \tag{1.62}$$

where the velocity gradient was adopted to set the work conjugacy as

$$\boldsymbol{\sigma} : \boldsymbol{D} = \boldsymbol{\sigma} : \boldsymbol{L} = \boldsymbol{\sigma} : \dot{\boldsymbol{F}}\boldsymbol{F}^{-1} = \boldsymbol{\sigma}\boldsymbol{F}^{-T} : \boldsymbol{F}. \tag{1.63}$$

Since the Clausius-Duhem inequality must hold for any thermokinetic process and so remain valid for any set $\{\dot{\boldsymbol{F}}(t), \dot{\theta}(t)\}$, the Cauchy stress and entropy constitutive equations must be

$$\boldsymbol{\sigma} = \rho\frac{\partial \psi}{\partial \boldsymbol{F}}\boldsymbol{F}^T, \tag{1.64}$$

$$s = -\frac{\partial \psi}{\partial \theta}. \tag{1.65}$$

It is also possible to write the constitutive equations for the Kirchhoff stress tensor as

$$\boldsymbol{\tau} = J\rho\frac{\partial \psi}{\partial \boldsymbol{F}}\boldsymbol{F}^T, \tag{1.66}$$

multiplying Equation (1.64) by J, and the first Piola-Kirchhoff stress tensor as

$$\boldsymbol{P} = \rho_0\frac{\partial \psi}{\partial \boldsymbol{F}} \tag{1.67}$$

multiplying Equation (1.62) also by J.

For each internal variable α_k of the set α of internal variables, the conjugate thermodynamical forces are defined to be

$$A_k \equiv \rho_0\frac{\partial \psi}{\partial \alpha_k}, \tag{1.68}$$

so that the Clausius-Duhem equation can be written in a reduced form as

$$-A * \dot{\boldsymbol{\alpha}} - \frac{J}{\theta}\boldsymbol{q}\cdot\boldsymbol{g} \geq 0, \tag{1.69}$$

where $\boldsymbol{A}$ is the set of conjugate thermodynamical forces and $*$ denotes the appropriate product operation.

To completely define the constitutive model, one still needs to postulate the constitutive equations for the flux variables $\dot{\boldsymbol{\alpha}}$ and $\frac{1}{\theta}\boldsymbol{q}$. These are given by

$$\dot{\boldsymbol{\alpha}} = f(\boldsymbol{F},\theta,\boldsymbol{g},\boldsymbol{\alpha}), \tag{1.70}$$

$$\frac{1}{\theta}\boldsymbol{q} = g(\boldsymbol{F},\theta,\boldsymbol{g},\boldsymbol{\alpha}). \tag{1.71}$$

A sufficient condition for the previous constitutive functions to satisfy the Clausius-Duhem inequality is the hypothesis of normal dissipativity, whereby one defines the constitutive functions for the flux variables as

$$\dot{\alpha}_k = -\frac{\partial \Xi}{\partial A_k}, \quad \frac{1}{\theta}\boldsymbol{q} = -\frac{\partial \Xi}{\partial \boldsymbol{g}}, \tag{1.72}$$

where the dissipation potential is

$$\Xi = \Xi(\boldsymbol{A},\boldsymbol{g};\boldsymbol{F},\theta,\boldsymbol{\alpha}), \tag{1.73}$$

a convex function with respect to each A_k and $\boldsymbol{g}$, and zero valued at the origin, $\{\boldsymbol{A},\boldsymbol{g}\} = \{\boldsymbol{0},\boldsymbol{0}\}$. Note that in the previous definition the state variables appear only as parameters.

Chapter 2

Mechanical problem

In the following chapter, the general framework presented in the previous chapter is applied to a purely mechanical analysis, neglecting the thermal terms.

2.0.1 Mechanical constitutive initial value problem

In the purely mechanical case, with all the quantities related to the thermal domain removed, a constitutive model based on internal variables is established by the following set of equations

$$\boldsymbol{P} = \rho_0 \frac{\partial \psi}{\partial \boldsymbol{F}}, \tag{2.1}$$

$$\psi = \psi(\boldsymbol{F}, \boldsymbol{\alpha}), \tag{2.2}$$

$$\dot{\boldsymbol{\alpha}} = f(\boldsymbol{F}, \boldsymbol{\alpha}). \tag{2.3}$$

Thus, the spatial mechanical constitutive initial value problem can be stated as follows

Problem 2.1 | Spatial mechanical constitutive initial value problem.

Given the initial values of the internal variables, $\boldsymbol{\alpha}(t_0)$, and the history of the deformation gradient

$$\boldsymbol{F}(t), \quad t \in [t_0, t_{\text{end}}], \tag{2.4}$$

find the functions for $\boldsymbol{\sigma}(t)$ and $\boldsymbol{\alpha}(t)$ such that the constitutive equations

$$\boldsymbol{\sigma} = \rho \frac{\partial \psi}{\partial \boldsymbol{F}} \boldsymbol{F}^T, \tag{2.5}$$

$$\psi = \psi(\boldsymbol{F}, \boldsymbol{\alpha}), \tag{2.6}$$

$$\dot{\boldsymbol{\alpha}} = f(\boldsymbol{F}, \boldsymbol{\alpha}). \tag{2.7}$$

are satisfied for every $t \in [t_0, t_{\text{end}}]$.

Likewise, in a material description it can be stated as

Problem 2.2 | Material mechanical constitutive intial value problem.

Given the initial values of the internal variables, $\boldsymbol{\alpha}(t_0)$, and the history of the deformation gradient

$$\boldsymbol{F}(t), \quad t \in [t_0, t_{\text{end}}], \tag{2.8}$$

find the functions for $\boldsymbol{P}(t)$ and $\boldsymbol{\alpha}(t)$ such that the constitutive equations

$$\boldsymbol{P} = \rho_0 \frac{\partial \psi}{\partial \boldsymbol{F}}, \tag{2.9}$$

$$\psi = \psi(\boldsymbol{F}, \boldsymbol{\alpha}), \tag{2.10}$$

$$\dot{\boldsymbol{\alpha}} = f(\boldsymbol{F}, \boldsymbol{\alpha}). \tag{2.11}$$

are satisfied for every $t \in [t_0, t_{\text{end}}]$.

2.0.2 Weak equilibrium. The principle of virtual work

The strong equations that enforce the equilirium of a body can be writen using the spatial description as

$$\rho \ddot{\boldsymbol{u}} = \operatorname{div} \boldsymbol{\sigma} + \boldsymbol{b} \quad \text{in } \Omega. \tag{2.12}$$

From a practical standpoint, finding the exact solution to the strong equilibrium equations in the context of real engineering problems is most often nearly or entirely impossible. Most numerical methods obtain only approximate solutions to the so-called weak equilibrium equations to circumvent this problem. These result from relaxing the strong equilibrium equations so that the solutions need only satisfy the equilibrium equations in an average sense instead of satisfying them pointwise. This is achieved through an integration over the body volume. The weak equilibrium equations can be found making use of several energetic and weighted residual methods, such as the Virtual Work Principle used here.

Problem 2.3 | Principle of virtual work (spatial version).

The Virtual Work Principle states, in a spatial description, that the body is in equilibrium if and only if the Cauchy stress field satisfies

$$\int_\Omega [\boldsymbol{\sigma} : \nabla \boldsymbol{\eta} - (\boldsymbol{b} - \rho \ddot{\boldsymbol{u}}) \cdot \boldsymbol{\eta}] \, \mathrm{d}v - \int_{\partial\Omega} \boldsymbol{t} \cdot \boldsymbol{\eta} \, \mathrm{d}a = 0, \quad \forall \boldsymbol{\eta} \in \mathscr{V}, \tag{2.13}$$

where $\mathscr{V}$ is the space of virtual displacement of the body, defined by the space of sufficiently regular arbitrary displacements

$$\boldsymbol{\eta} \colon \Omega \to \mathscr{U} \tag{2.14}$$

where $\mathscr{U}$ is the n-dimension vector associated with $\mathscr{E}$.

The principle of virtual work can be expressed in a completly equivalent way using a material description.

Problem 2.4 | Principle of virtual work (material version).

The Virtual Work Principle states, in a material description, that the body is in

equilibrium if and only if the First Piola-Kirchhoff stress field satisfies

$$\int_{\Omega_0} [\boldsymbol{P} : \nabla_0 \boldsymbol{\eta} - (\boldsymbol{b}_0 - \rho_0 \ddot{\boldsymbol{u}}) \cdot \boldsymbol{\eta}] \, \mathrm{d}v - \int_{\partial\Omega_0} \boldsymbol{t}_0 \cdot \boldsymbol{\eta} \, \mathrm{d}da = 0, \quad \forall \boldsymbol{\eta} \in \mathscr{V}, \tag{2.15}$$

where $\mathscr{V}$ is the space of virtual displacement of the body, defined by the space of sufficiently regular arbitrary displacements

$$\boldsymbol{\eta} : \Omega \to \mathscr{U}. \tag{2.16}$$

2.0.3 Mechanical constitutive initial boundary value problem

It is now possible to pose the mechanical constitutive initial value problem in its weak form. Assume that a body $\mathscr{B}$ is made from a generic material, characterized by a given constitutive model, whose internal variables are known at the initial time, as presented in Figure **??**. In addition, it is assumed that the interior of the body was subjected to a prescribed history of body forces, $\boldsymbol{b}(\boldsymbol{X}, t)$, $t \in [t_0, t_{\text{end}}]$, and to the following boundary conditions:

- **Natural (or Neumann) boundary condition:** The boundary portion $\Omega_{\text{traction, 0}}$ of $\mathscr{B}$ is subjected to a prescribed history of traction forces, $\boldsymbol{t}_{\text{presc}}(\boldsymbol{X}, t)$, $\boldsymbol{X} \in \partial\Omega_{\text{traction},0}$, $t \in [t_0, t_{\text{end}}]$,

- **Essential (or Dirichlet) boundary condition:** The boundary portion $\Omega_{\text{motion, 0}}$ of $\mathscr{B}$ is subjected to a prescribed displacement field history, $\boldsymbol{u}_{\text{presc}}(\boldsymbol{X}, t)$, such that

$$\boldsymbol{\varphi}(\boldsymbol{X}, t) = \boldsymbol{X} + \boldsymbol{u}_{\text{presc}}(\boldsymbol{X}, t), \quad \boldsymbol{X} \in \partial\Omega_{\text{motion, 0}}, \quad t \in [t_0, t_{\text{end}}].$$

It is also convenient to define the set of kinematically admissible displacements of $\mathscr{B}$ as the set of all sufficiently regular displacement functions tha satisfy the essential boundary condition (**?**),

$$\mathscr{K} \equiv \{\boldsymbol{u} : \Omega \times \mathscr{R} \to \mathscr{U} \mid \boldsymbol{u}(\boldsymbol{X}, t) = \boldsymbol{u}_{\text{presc}}(\boldsymbol{X}, t), \quad \boldsymbol{X} \in \partial\Omega_{\text{motion},0}, \quad t \in [t_0, t_{\text{end}}]\}. \tag{2.17}$$

So the weak form of the quasi-static mechanical constitutive initial boundary value problem can be stated in a spatial description as follows

Problem 2.5 | Spatial mechanical initial BVP.

Find a kinematically admissible displacement function, $\boldsymbol{u} \in \mathscr{K}$, such that for every $t \in [t_0, t_{\text{end}}]$, the body $\mathscr{B}$ is in equilibrium as stated by the Virtual Work Principle

$$\int_{\Omega} [\boldsymbol{\sigma} : \nabla \boldsymbol{\eta} - (\boldsymbol{b} - \rho \ddot{\boldsymbol{u}}) \cdot \boldsymbol{\eta}] \, \mathrm{d}v - \int_{\partial\Omega} \boldsymbol{t} \cdot \boldsymbol{\eta} \, \mathrm{d}a = 0, \quad \forall \boldsymbol{\eta} \in \mathscr{V}, \tag{2.18}$$

where the space of virtual displacements at time t is defined by

$$\mathscr{V} \equiv \left\{\boldsymbol{\eta} : \Omega \to \mathscr{U} \mid \boldsymbol{\eta} = \boldsymbol{0} \quad \text{in} \quad \partial\Omega_{\text{motion},0}\right\}, \tag{2.19}$$

and at each point of $\mathscr{B}$, the Cauchy stress tensor is the solution of spatial mechanical constitutive initial values problem.

and in the material description as

Problem 2.6 | Material mechanical initial BVP.

Find a kinematically admissible displacement function, $\boldsymbol{u} \in \mathscr{K}$, such that for every $t \in [t_0, t_{\text{end}}]$, the body $\mathscr{B}$ is in equilibrium as stated by the Virtual Work Principle

$$\int_{\Omega_0} [\boldsymbol{P} : \nabla_0 \boldsymbol{\eta} - (\boldsymbol{b}_0 - \rho_0 \ddot{\boldsymbol{u}}) \cdot \boldsymbol{\eta}] \, \mathrm{d}v - \int_{\partial\Omega_0} \boldsymbol{t}_0 \cdot \boldsymbol{\eta} \, \mathrm{d}a = 0, \quad \forall \boldsymbol{\eta} \in \mathscr{V}, \tag{2.20}$$

where the space of virtual displacements at time t is defined by

$$\mathscr{V} \equiv \left\{ \boldsymbol{\eta} : \Omega_0 \to \mathscr{U} \mid \boldsymbol{\eta} = \boldsymbol{0} \quad \text{in} \quad \partial\Omega_{\text{motion},0} \right\}, \tag{2.21}$$

and at each point of $\mathscr{B}$, the First Piola-Kirchhoff stress tensor is the solution of material mechanical constitutive initial values problem.

2.1 Time descretization

Given a generic path-dependent model, i.e., a model in which the stress state does not depend only on the instantaneous deformation state but also on the deformation history, the solution of the constitutive initial value problem for a given set of initial conditions is usually not known for complex strain paths $\boldsymbol{F}(t)$. Thus, there is a need to use an appropriate numerical algorithm to integrate the rate constitutive equations.

In general, the algorithms for integrating rate constitutive equations are obtained adopting some time (or pseudo-time) discretization and some hypothesis on the deformation path between adjacent time stations. In the present document, an algorithm is adopted based on approximated incremental constitutive functions. Attending to the mechanical constitutive initial boundary value problem and considering the time increment $[t_n, t_{n+1}]$, this approach is comprised by the following two requirements:

- **Cauchy and First Piola-Kirchhoff stress tensors.** Considering a time increment $[t_n, t_{n+1}]$ and given the set $\boldsymbol{\alpha}_n$ of internal variables at t_n, the deformation gradient $\boldsymbol{F}_{n+1}$ at time t_{n+1} determines the stress $\boldsymbol{\sigma}_{n+1}$ uniquely through

$$\boldsymbol{\sigma}_{n+1} = \hat{\boldsymbol{\sigma}}(\boldsymbol{\alpha}_n, \boldsymbol{F}_{n+1}), \tag{2.22}$$

  where $\hat{\boldsymbol{\sigma}}$ is the incremental constitutive function for the Cauchy stress tensor.

  Similarly, the First Piola-Kirchhoff stress tensor $\boldsymbol{P}_{n+1}$ must be uniquely determined by the prescribed deformation gradient $\boldsymbol{F}_{n+1}$ prescribed at t_{n+1} as

$$\boldsymbol{P}_{n+1} = \hat{\boldsymbol{P}}(\boldsymbol{\alpha}_n, \boldsymbol{F}_{n+1}), \tag{2.23}$$

  where $\hat{\boldsymbol{P}}$ is the incremental constitutive function for the First Piola-Kirchhoff stress tensor.

- **Set of internal variables.** Assuming that the set of internal variables $\boldsymbol{\alpha}_n$ is known at t_n, the set of internal variables must be uniquely determined by the prescribed deformationgradient $\boldsymbol{F}_{n+1}$ prescribed at t_{n+1} as

$$\boldsymbol{\alpha}_{n+1} = \hat{\boldsymbol{\alpha}}(\boldsymbol{\alpha}_n, \boldsymbol{F}_{n+1}), \tag{2.24}$$

  where $\hat{\boldsymbol{\alpha}}$ is the incremental constitutive function for the set of internal variables.

Generally, the numerical constitutive laws are nonlinear and path-independent within one increment. In other words, within each increment, $\boldsymbol{\sigma}_{n+1}$ and $\boldsymbol{\alpha}_{n+1}$, they are functions of $\boldsymbol{F}_{n+1}$ alone with the argument $\boldsymbol{\alpha}_n$ constant within the same time interval.

Making use of the aforementioned time discretization, one can state the weak form of the mechanical constitutive initial boundary value problem in the spatial description as

Problem 2.7 | Spatial incremental mechanical initial BVP.

Given the set of internal variables $\boldsymbol{\alpha}_n$ at t_n, the prescribed body and traction force fields $\boldsymbol{b}_{n+1}$ and $\boldsymbol{t}_{n+1}$ at t_{n+1}, and the prescribed deformating gradient $\boldsymbol{F}_{n+1}$ at t_{n+1}, find the kinematically admissible displacement field $\boldsymbol{u}_{n+1} \in \mathscr{K}_{n+1}$ such that the body $\mathscr{B}$ is in equilibrium as stated by the virtual Work Principle

$$\int_{\Omega_{n+1}} [\hat{\boldsymbol{\sigma}}(\boldsymbol{F}_{n+1}, \boldsymbol{\alpha}_n) : \nabla\boldsymbol{\eta} - (\boldsymbol{b}_{n+1} - \rho\ddot{\boldsymbol{u}}_{n+1}) \cdot \boldsymbol{\eta}] \, \mathrm{d}v - \int_{\partial\Omega_{n+1}} \boldsymbol{t}_{n+1} \cdot \boldsymbol{\eta} \, \mathrm{d}a = 0, \quad \forall \boldsymbol{\eta} \in \mathscr{V}, \tag{2.25}$$

where the space of kinematically admissible displacement fields $\mathscr{K}_{n+1}$ is defined by

$$\mathscr{K}_{n+1} \equiv \{\boldsymbol{u} : \Omega \times \mathscr{R} \to \mathscr{U} \mid \boldsymbol{u}_{n+1}(\boldsymbol{X}) = \boldsymbol{u}_{\mathrm{presc},n+1}(\boldsymbol{X}),\ \boldsymbol{X} \in \partial\Omega_{\mathrm{motion},0}\}. \tag{2.26}$$

and in the material description as

Problem 2.8 | Material incremental mechanical initial BVP.

Given the set of internal variables $\boldsymbol{\alpha}_n$ at t_n, the prescribed body and traction force fields $\boldsymbol{b}_{0,n+1}$ and $\boldsymbol{t}_{0,n+1}$ at t_{n+1}, and the prescribed deformating gradient $\boldsymbol{F}_{n+1}$ at t_{n+1}, find the kinematically admissible displacement field $\boldsymbol{u}_{n+1} \in \mathscr{K}_{n+1}$ such that the body $\mathscr{B}$ is in equilibrium as stated by the virtual Work Principle

$$\int_{\Omega_{n+1}} [\hat{\boldsymbol{P}}(\boldsymbol{F}_{n+1}, \boldsymbol{\alpha}_n) : \nabla_0\boldsymbol{\eta} - (\boldsymbol{b}_{0,n+1} - \rho_0\ddot{\boldsymbol{u}}_{n+1}) \cdot \boldsymbol{\eta}] \, \mathrm{d}v - \int_{\partial\Omega_{n+1}} \boldsymbol{t}_{0,n+1} \cdot \boldsymbol{\eta} \, \mathrm{d}a = 0, \quad \forall \boldsymbol{\eta} \in \mathscr{V}, \tag{2.27}$$

where the space of kinematically admissible displacement fields $\mathscr{K}_{n+1}$ is defined by

$$\mathscr{K}_{n+1} \equiv \{\boldsymbol{u} : \Omega \times \mathscr{R} \to \mathscr{U} \mid \boldsymbol{u}_{n+1}(\boldsymbol{X}) = \boldsymbol{u}_{\mathrm{presc},n+1}(\boldsymbol{X}),\ \boldsymbol{X} \in \partial\Omega_{\mathrm{motion},0}\}. \tag{2.28}$$

2.2 Finite Element Method

With the incremental weak form of the mechanical constitutive initial boundary value problem now established, an approximated solution can be found using the Finite Element Method.

2.2.1 Finite element concept

The first in the Finite Element method is to discretize the continuum domain Ω in a finite set of n_{elem} mutually exclusive subdomains called finite elements $\Omega^{(e)}$. The discretized domain, ${}^h\Omega$, is therefore an approximation to the continuum domain expressed by

$$\Omega \approx^h \Omega \equiv \bigcup_{e=1}^{n_{\text{elem}}} \Omega^{(e)}. \tag{2.29}$$

The space of virtual displacements $\mathscr{V}$ as well as the space of kinematically admissible displacement fields $\mathscr{K}$ are also discretized in the same, with their discretized forms denoted by ${}^h\mathscr{V}$ and ${}^h\mathscr{K}$.

2.2.2 Interpolation functions

Let e be a generic finite element with n_{nodes} nodes, where each node i of coordinates $\boldsymbol{x}^i$ is associated with an interpolation function $N_i^{(e)}$. These interpolation functions are often called shape functions and perform the required filed interpolations inside the element domain $\Omega^{(e)}$.

Letting $a(\boldsymbol{x})$ be a generic field defined over $\Omega^{(e)}$, its interpolation at any point $\boldsymbol{x}$ inside the element is defined by the element shape functions as

$$a(\boldsymbol{x}) \approx^h a(\boldsymbol{x}) \equiv \sum_{i=1}^{n_{\text{nodes}}} a(\boldsymbol{x}_i) N_i^{(e)}(\boldsymbol{x}). \tag{2.30}$$

If instead $a(\boldsymbol{x})$ is instead a generic field defined over the global domain Ω, the interpolation of $a(\boldsymbol{x})$ at any point $\boldsymbol{x}$ is defined by the global shape functions as

$$a(\boldsymbol{x}) \approx^h a(\boldsymbol{x}) \equiv \sum_{i=1}^{n_{\text{points}}} a(\boldsymbol{x}_i) N_i^{g}(\boldsymbol{x}), \tag{2.31}$$

where n_{points} is the total number of nodes of the finite element mesh. The discretized spaces ${}^h\mathscr{V}$ and ${}^h\mathscr{K}$ can now be defined as

$${}^h\mathscr{K} \equiv \left\{ {}^h\boldsymbol{u}(\boldsymbol{x}) = \sum_{i=1}^{n_{\text{points}}} \boldsymbol{u}(\boldsymbol{x}_i) N_i^{g}(\boldsymbol{x}) \mid \boldsymbol{u}(\boldsymbol{x}_i) = \boldsymbol{u}_{\text{presc}}(\boldsymbol{x}_i) \quad \text{if } \boldsymbol{x}_i \in \partial\Omega_{\text{motion},0} \right\}, \tag{2.32}$$

$${}^h\mathscr{V} \equiv \left\{ {}^h\boldsymbol{\eta}(\boldsymbol{x}) = \sum_{i=1}^{n_{\text{points}}} \boldsymbol{\eta}(\boldsymbol{x}_i) N_i^{g}(\boldsymbol{x}) \mid \boldsymbol{\eta}(\boldsymbol{x}_i) = \boldsymbol{0} \quad \text{if } \boldsymbol{x}_i \in \partial\Omega_{\text{motion},0} \right\} \tag{2.33}$$

2.2.3 Interpolation matrix and discrete gradient operators

The global shape functions can be conveniently assembled in the so-called global interpolation matrix as

$$\mathbf{N}^g(\boldsymbol{x}) \equiv \left[\mathrm{diag}[N_1^g(\boldsymbol{x})]\ \mathrm{diag}[N_2^g(\boldsymbol{x})]\ \cdots\ \mathrm{diag}[N_{n_{\mathrm{points}}}^g(\boldsymbol{x})]\right], \tag{2.34}$$

where $\mathrm{diag}[N_i^g]$ is a diagonal matrix $n_{\mathrm{dim}} \times n_{\mathrm{dim}}$

$$\mathrm{diag}[N_i^g(\boldsymbol{x})] \equiv \begin{bmatrix} N_i^g & 0 & \cdots & 0 \\ 0 & N_i^g & \cdots & 0 \\ \vdots & \vdots & \ddots & \vdots \\ 0 & 0 & \cdots & N_i^g \end{bmatrix} \tag{2.35}$$

where n_{dim} is the number of degrees of freedom per node.

Defining the global vector of nodal displacements as

$$\mathbf{u} = \left[u_1^1, \ldots, u_{n_{\mathrm{dim}}}^1, \ldots, u_1^{n_{\mathrm{points}}}, \ldots, u_{n_{\mathrm{dim}}}^{n_{\mathrm{points}}}\right]^T, \tag{2.36}$$

the displacement field $\vec{u}(\boldsymbol{x})$m defined over the global domain Ω, can be found from Equation (2.31) at any point $\boldsymbol{x}$ as

$$^h\boldsymbol{u}(\boldsymbol{x}) \equiv \mathbf{N}^g(\boldsymbol{x})\mathbf{u}, \quad ^h\boldsymbol{u} \in {}^h\mathscr{K}. \tag{2.37}$$

2.2.4 Spatial discretization

Applying the aforementioned finite element discretization to the incremental mechanical constitutive initial boundary value problem, we can then write in the spatial description

$$\int_{^h\Omega} \left[\hat{\boldsymbol{\sigma}}^T \mathbf{B}^g \boldsymbol{\eta} - (\mathbf{b}_{n+1} - \rho\ddot{\mathbf{u}}_{n+1}) \cdot \mathbf{N}^g \boldsymbol{\eta}\right] \mathrm{d}v - \int_{\partial^h\Omega_{\mathrm{traction}}} \mathbf{t}_{n+1} \cdot \mathbf{N}^g \boldsymbol{\eta}\, \mathrm{d}a = 0, \quad \forall \boldsymbol{\eta} \in {}^h\mathscr{V}, \tag{2.38}$$

where $\mathbf{B}^g$ is the discrete symmetric global gradient operator, defined for a 2D problem in cartesian coordinates as

$$\mathbf{B}^g \equiv \begin{bmatrix} \frac{\partial N_1^g}{\partial x} & 0 & \frac{\partial N_2^g}{\partial x} & 0 & \cdots & \frac{\partial N_{n_{\mathrm{points}}}^g}{\partial x} & 0 \\ 0 & \frac{\partial N_1^g}{\partial y} & 0 & \frac{\partial N_2^g}{\partial y} & \cdots & 0 & \frac{\partial N_{n_{\mathrm{points}}}^g}{\partial y} \\ \frac{\partial N_1^g}{\partial y} & \frac{\partial N_1^g}{\partial x} & \frac{\partial N_2^g}{\partial y} & \frac{\partial N_2^g}{\partial x} & \cdots & \frac{\partial N_{n_{\mathrm{points}}}^g}{\partial y} & \frac{\partial N_{n_{\mathrm{points}}}^g}{\partial x} \end{bmatrix}. \tag{2.39}$$

Equation (4.39) can be rewritten as

$$\left\{\int_{^h\Omega} \left[\mathbf{B}^{gT} \hat{\boldsymbol{\sigma}}(\boldsymbol{\alpha}_n, \boldsymbol{F}_{n+1}) - \mathbf{N}^{gT}\mathbf{b}_{n+1} + \mathbf{N}^{gT}\rho\ddot{\mathbf{u}}_{n+1}\right] \mathrm{d}v - \int_{\partial^h\Omega_{\mathrm{traction}}} \mathbf{N}^{gT}\mathbf{t}_{n+1}\, \mathrm{d}a\right\}^T \boldsymbol{\eta} = 0, \quad \forall \boldsymbol{\eta} \in {}^h\mathscr{V}, \tag{2.40}$$

and, since it must be satisfied for any $\boldsymbol{\eta} \in {}^{h}\mathscr{V}$, the incremental quasi-static discretized mechanical constitutive initial boundary value problem can thus be stated in the spatial description as

Problem 2.9 | Spatial incremental discretized mechanical initial BVP.

Given the set of internal variables $\boldsymbol{\alpha}_n$ at t_n, the prescribed body and traction force fields $\boldsymbol{b}_{n+1}$ and $\boldsymbol{t}_{n+1}$, and the prescribed deformation gradient $\boldsymbol{F}_{n+1}$ at t_{n+1}, find the kinematically admissible nodal displacement field $\boldsymbol{u}_{n+1} \in {}^{h}\mathscr{K}_{n+1}$ such that the body $\mathscr{B}$ is in equilibrium as stated by the Virtual Work Principle

$$\mathbf{M}\ddot{\mathbf{u}}_{n+1} + \mathbf{f}^{\text{int}}(\mathbf{u}_{n+1}) - \mathbf{f}^{\text{ext}}_{n+1} = \mathbf{0}, \tag{2.41}$$

where $\mathbf{f}^{\text{int}}$ e $\mathbf{f}^{\text{ext}}_{n+1}$ are the global vectors of internal and external forces defined as

$$\mathbf{f}^{\text{int}} \equiv \int_{{}^{h}\Omega} \mathbf{B}^{g\,T} \hat{\boldsymbol{\sigma}}(\boldsymbol{F}_{n+1}, \boldsymbol{\alpha}_n)\, \mathrm{d}v, \tag{2.42}$$

$$\mathbf{f}^{\text{ext}}_{n+1} \equiv \int_{{}^{h}\Omega} \mathbf{N}^{g\,T} \mathbf{b}_{n+1}\, \mathrm{d}v + \int_{\partial {}^{h}\Omega_{\text{traction}}} \mathbf{N}^{g\,T} \mathbf{t}_{n+1}\, \mathrm{d}a, \tag{2.43}$$

and $\mathbf{M}$ is the mass matrix defined as

$$\mathbf{M} = \int_{{}^{h}\Omega} \rho \mathbf{N}^{g\,T}\, \mathrm{d}v. \tag{2.44}$$

In a material description, Equation (4.41) is written as

$$\left\{ \int_{{}^{h}\Omega_0} \left[\mathbf{G}^{g\,T} \hat{\boldsymbol{P}}(\boldsymbol{\alpha}_n, \boldsymbol{F}_{n+1}) - \mathbf{N}^{g\,T} \mathbf{b}_{0,n+1} + \mathbf{N}^{g\,T} \rho_0 \ddot{\mathbf{u}}_{n+1} \right] \mathrm{d}v \right.$$
$$\left. - \int_{\partial {}^{h}\Omega_{\text{traction},0}} \mathbf{N}^{g\,T} \mathbf{t}_{0,n+1}\, \mathrm{d}a \right\}^{T} \boldsymbol{\eta} = 0, \quad \forall \boldsymbol{\eta} \in {}^{h}\mathscr{V}, \tag{2.45}$$

where $\mathbf{G}^g$ is the discrete global gradient operator, defined for a 2D problem in cartesian coordinates as

$$\mathbf{G}^g \equiv \begin{bmatrix} \dfrac{\partial N^g_1}{\partial x} & 0 & \dfrac{\partial N^g_2}{\partial x} & 0 & \cdots & \dfrac{\partial N^g_{n_{\text{points}}}}{\partial x} & 0 \\ 0 & \dfrac{\partial N^g_1}{\partial x} & 0 & \dfrac{\partial N^g_2}{\partial x} & 0 & \cdots & \dfrac{\partial N^g_{n_{\text{points}}}}{\partial x} \\ \dfrac{\partial N^g_1}{\partial y} & 0 & \dfrac{\partial N^g_2}{\partial y} & \cdots & 0 & \dfrac{\partial N^g_{n_{\text{points}}}}{\partial y} & 0 \\ 0 & \dfrac{\partial N^g_1}{\partial y} & 0 & \dfrac{\partial N^g_2}{\partial y} & \cdots & 0 & \dfrac{\partial N^g_{n_{\text{points}}}}{\partial y} \end{bmatrix}, \tag{2.46}$$

and, as for the spatial description, it must be satisfied for any $\boldsymbol{\eta} \in {}^{h}\mathscr{V}$, the incremental quasi-static discretized mechanical constitutive initial boundary value problem can thus be stated in the material description as

Problem 2.10 | Material incremental discretized mechanical initial BVP.

Given the set of internal variables $\boldsymbol{\alpha}_n$ at t_n, the prescribed body and traction force fields $\boldsymbol{b}_{0,n+1}$ and $\boldsymbol{t}_{0,n+1}$, and the prescribed deformation gradient $\boldsymbol{F}_{n+1}$ at t_{n+1}, find the kinematically admissible nodal displacement field $\boldsymbol{u}_{n+1} \in {}^h\mathscr{K}_{n+1}$ such that the body $\mathscr{B}$ is in equilibrium as stated by the Virtual Work Principle

$$\mathbf{M}\ddot{\mathbf{u}}_{n+1} + \mathbf{f}^{\text{int}}(\mathbf{u}_{n+1}) - \mathbf{f}^{\text{ext}}_{n+1} = \mathbf{0}, \tag{2.47}$$

where $\mathbf{f}^{\text{int}}$ e $\mathbf{f}^{\text{ext}}_{n+1}$ are the global vectors of internal and external forces defined as

$$\mathbf{f}^{\text{int}} \equiv \int_{{}^h\Omega_0} \mathbf{G}^{g\,T}\hat{\boldsymbol{P}}(\boldsymbol{F}_{n+1}, \boldsymbol{\alpha}_n)\,\mathrm{d}v, \tag{2.48}$$

$$\mathbf{f}^{\text{ext}}_{n+1} \equiv \int_{{}^h\Omega_0} \mathbf{N}^{g\,T}\mathbf{b}_{0,n+1}\,\mathrm{d}v + \int_{\partial^h\Omega_{\text{traction},0}} \mathbf{N}^{g\,T}\mathbf{t}_{0,n+1}\,\mathrm{d}a. \tag{2.49}$$

and $\mathbf{M}$ is the mass matrix defined as

$$\mathbf{M} = \int_{{}^h\Omega_0} \rho_0 \mathbf{N}^{g\,T}\mathbf{N}^{g}\,\mathrm{d}v. \tag{2.50}$$

The global vectors for the internal and external forces are usually obtained by assemblage of their elemental counterparts as

$$\mathbf{f}^{\text{int}} = \mathop{\mathsf{A}}_{e=1}^{n_{\text{elem}}} \left(\mathbf{f}^{\text{int}}\right)^{(e)}, \tag{2.51}$$

$$\mathbf{f}^{\text{ext}} = \mathop{\mathsf{A}}_{e=1}^{n_{\text{elem}}} \left(\mathbf{f}^{\text{ext}}\right)^{(e)}, \tag{2.52}$$

where the elemental vectors in the spatial description are defined as

$$\left(\mathbf{f}^{\text{int}}\right)^{(e)} \equiv \int_{{}^h\Omega^{(e)}} \mathbf{B}^{T}\hat{\boldsymbol{\sigma}}(\boldsymbol{F}_{n+1}, \boldsymbol{\alpha}_n)\,\mathrm{d}v, \tag{2.53}$$

$$\left(\mathbf{f}^{\text{ext}}_{n+1}\right)^{(e)} \equiv \int_{{}^h\Omega^{(e)}} \mathbf{N}^{T}\mathbf{b}_{n+1}\,\mathrm{d}v + \int_{\partial^h\Omega^{(e)}_{\text{traction}}} \mathbf{N}^{T}\mathbf{t}_{n+1}\,\mathrm{d}a, \tag{2.54}$$

and in material description as

$$\left(\mathbf{f}^{\text{int}}\right)^{(e)} \equiv \int_{{}^h\Omega^{(e)}_0} \mathbf{G}^{T}\hat{\boldsymbol{P}}(\boldsymbol{F}_{n+1}, \boldsymbol{\alpha}_n)\,\mathrm{d}v, \tag{2.55}$$

$$\left(\mathbf{f}^{\text{ext}}_{n+1}\right)^{(e)} \equiv \int_{{}^h\Omega^{(e)}_0} \mathbf{N}^{T}\mathbf{b}_{0,n+1}\,\mathrm{d}v + \int_{\partial^h\Omega^{(e)}_{0,\text{ traction}}} \mathbf{N}^{T}\mathbf{t}_{0,n+1}\,\mathrm{d}a, \tag{2.56}$$

The matrices $\mathbf{N}$, $\mathbf{B}$, and $\mathbf{G}$ are the elemental interpolation matrix, the symmetric elemental gradient operator, and the discrete elemental gradient operator.

In a similar manner, the global mass matrix is also usually obtained by assemblage of their elemental counterparts as

$$\mathbf{M} \equiv \mathop{\mathsf{A}}_{e=1}^{n_{\text{elem}}} \mathbf{M}^{(e)}, \tag{2.57}$$

where the elemental mass matrices in the spatial description are defined as

$$\mathbf{M}^{(e)} = \int_{h\Omega^{(e)}} \rho \mathbf{N}^T \mathbf{N} \, \mathrm{d}v, \tag{2.58}$$

and the material descriptrion

$$\mathbf{M}^{(e)} = \int_{h\Omega_0^{(e)}} \rho_0 \mathbf{N}^T \mathbf{N} \, \mathrm{d}v. \tag{2.59}$$

2.2.5 Numerical integration

In the Finite Element Method, the integrations over the element domain are generally performed numerically using the Gaussian Quadrature Method. Stating it's application succinctly, let $a(\boldsymbol{x})$ be a generic field, if there is a coordinate transformation from a local (or natural) normalized domain Υ to the element domain $\Omega^{(e)}$, $\boldsymbol{x}\colon \Upsilon \to \Omega^{(e)}$, the integral of $a(\boldsymbol{x})$ over the domain $\Omega^{(e)}$ can be numerically determined as

$$\int_{\Omega^{(e)}} a(\boldsymbol{x}) \, \mathrm{d}\boldsymbol{x} = \int_{\Upsilon} a(\boldsymbol{x}(\boldsymbol{\zeta})) \, j(\boldsymbol{\zeta}) \, \mathrm{d}\boldsymbol{\zeta} \approx \sum_{i=1}^{n_{\mathrm{GP}}} w_i \, a(\boldsymbol{x}(\boldsymbol{\zeta}_i)) \, j(\boldsymbol{\zeta}_i), \tag{2.60}$$

where $\boldsymbol{\zeta}_i$ and w_i, $i = 1, \ldots, n_{\mathrm{GP}}$ are the positions and weigths of the Gauss sampling points in the domain Υ and $j(\boldsymbol{\zeta})$ is the determinant of the coordinate trasnformation's Jacobian defined as

$$j(\boldsymbol{\zeta}) = \det\left(\frac{\partial \boldsymbol{x}}{\partial \boldsymbol{\zeta}}\right). \tag{2.61}$$

2.3 Linearisation

The equilibrium equation, Equation (2.41) in a spatial description and Equation (3.22) in a material description, is generally nonlinear due to geometrical and/or material nonlinearities. The Newton-Raphson Method is an efficient and robust iterative scheme with a quadratic convergence rate often used to solve the equilibrium equation at each time increment, t_n. The residual of the fully discretized balance of linear momentum is defined for an iteration step i of the Newton-Raphson method as

$$\mathbf{r}(\mathbf{u}_{n+1}^i) = \mathbf{M}\ddot{\mathbf{u}}_{n+1}^i + \mathbf{f}^{\mathrm{int}}(\mathbf{u}_{n+1}^i) - \mathbf{f}_{n+1}^{\mathrm{ext}}. \tag{2.62}$$

A Taylor expansion about the current solution $\mathbf{u}_{n+1}^i$ is performed, discarding all terms of higher order than one, yielding the linearised form

$$\mathrm{Lin}\,\mathbf{r}(\mathbf{u}_{n+1}^i) = \mathbf{r}(\mathbf{u}_{n+1}^i) + \underbrace{\left.\frac{\partial \mathbf{r}(\mathbf{u}_{n+1})}{\partial \mathbf{u}_{n+1}}\right|^i}_{\mathbf{K}(\mathbf{u}_{n+1}^i)} \delta\mathbf{u}. \tag{2.63}$$

with the dynamic effective tangential stiffness matrix $\mathbf{K}(\mathbf{u}_{n+1}^i)$. The linearisation of the internal forces included in $\mathbf{K}$ is known as the tangential stiffness matrix $\mathbf{K}_T$, which is defined as

$$\mathbf{K}_T^i = \left.\frac{\partial \mathbf{f}^{\mathrm{int}}}{\partial \mathbf{u}_{n+1}}\right|^i. \tag{2.64}$$

Equilibrium is achieved if

$$\mathrm{Lin}\,\mathbf{r}(\mathbf{u}_{n+1}^{i}) = \mathbf{0}, \tag{2.65}$$

so that a linear system of equation is given by

$$\mathbf{K}(\mathbf{u}_{n+1}^{i})\delta\mathbf{u} = -\mathbf{r}\left(\mathbf{u}_{n+1}^{i}\right). \tag{2.66}$$

Thus, a new solution of the displacement increment $\delta\mathbf{u}$ for current iteration step $i+1$ is determined, and the final displacement solution of time step $n+1$ is obtained via updating

$$\mathbf{u}_{n+1}^{i+1} = \mathbf{u}_{n+1}^{i} + \delta\mathbf{u}. \tag{2.67}$$

A solution of t_{n+1} is found, i.e. an equilibrium state is reached and $\mathbf{u}_{n+1} = \mathbf{u}_{n+1}^{i+1}$, if prescribed, user-defined convergence criteria are fulfilled.

2.4 Constitutive laws

Chapter 3

Thermo field

For the development of the thermomechanical models, appropriate for the target application to rocket nozzles, the temperature field needs to be considered. This section provides an overview of the governing equations required to describe a temperature field with the finite element method (FEM). A more detailed representation on this topic can be found in the literature, e.g. in Holzapfel [58], Lemaitre and Chaboche [78], and Polifke and Kopitz [105]. The procedure to establish a fully discrete system of equations for the themal field is comparable to the one for the structural field in chapter 3. Moreover, the basics of nonlinear continuum thermodynamics have already been featured in chapter 2. Consequently, the detailed derivation are skipped in this chapter.

In a first step, the balance equations for the thermal field will be established. Then, in a second step the thermal initial boundary value problem (IBVP) will be presented followed by the numerical solution technique. Latter requires a weak form of the thermal balance equation which will be fully discretised using the FEM for space discretisation and the finite difference method for time discretisation. To finish, the residual and the tangential system matrix will be introduced to enable the application of a Newton-Raphson method.

3.1 Governing equations

Based on the general model presented in Section **??**, the balance equations for the temperature field are obtained as a special case by neglecting all mechanical terms. Hence, the energy balance equation (Equation (1.41)), now in material description, reduces to

$$\rho_0 \; e = -\operatorname{div}_0 \boldsymbol{q}_0 + \rho_0 r \quad \text{in } \Omega_0, \tag{3.1}$$

where all mechanical terms are neglected. The target application of the present work is on coupled generally nonlinear thermomechanical interaction problems, where the initial and the current domains are not equal, i.e. $\Omega_0 \neq \Omega$. Thus, for the sake of simplicity and in view of the later coupled problem, all following relations are expressed in material quantities. A purely thermal analysis is independent of the deformation, so that reference and current configuration are identical and the domain remains constant, i.e. $\Omega_0 \equiv \Omega$.

3.2 Thermal constitutive initial value problem

From Section **??**, discarding all variables related to the mechanical problem, the general thermal constitutive initial value problem is

Problem 3.1 | General thermal constitutive intial value problem.

Given the initial value of the internal variables $\boldsymbol{\alpha}(t_0)$ and the history of the temperature distribution

$$\theta(t), \quad t \in [t_0, t_{\text{end}}],$$

find the function for $\boldsymbol{q}(t)$, $s(t)$ and $\boldsymbol{\alpha}(t)$ such that the constitutive equations

$$s = -\frac{\partial \psi}{\partial \theta}, \tag{3.2}$$

$$\psi = \psi(\theta), \tag{3.3}$$

$$\dot{\boldsymbol{\alpha}} = f(\theta, \boldsymbol{g}_0, \boldsymbol{\alpha}), \tag{3.4}$$

$$\frac{1}{\theta}\boldsymbol{q}_0 = g(\theta, \boldsymbol{g}_0, \boldsymbol{\alpha}). \tag{3.5}$$

are satisfied for every $t \in [t_0, t_{\text{end}}]$.

No distinction between spatial and material configurations applies as $\Omega = \Omega_0$.

Next, a standard set of assumptions are introduced. As a first step, the specific heat C_V is established and defined according to the thermodynamical principles to be the amount of heat required to change a unit mass of a substance by one degree in temperature, i.e.

$$C_{\text{V}} = \frac{\partial e}{\partial \theta}. \tag{3.6}$$

The index $(\cdot)_{\text{V}}$ denotes that C_{V} is measured at constant volume. Its dimensions are energy over temperature, i.e., $[\text{E}/\Theta]$, and using the International System of Units (SI), C_V is expressed in joules per kelvin. Using Equation 1.49, the specific heat at constant volume can be written as

$$C_{\text{V}} = -\frac{\partial^2 \psi}{\partial \theta^2}\theta = \frac{\partial s}{\partial \theta}\theta. \tag{3.7}$$

In general, the heat capacity depends on the deformation and on the temperature. A substance whose specific volume (or density) is constant is called an incompressible substance. This incompressibilty or constant-volume assumption should be taken to imply that the energy associated with the volume change is negligible compared with other forms of energy. For the application to elastomers, see for instance Netz [96], the heat capacity C_V can be assumed to depend only on the temperature, and the partial derivatives in Equation (3.7) turn into exact derivatives, yielding

$$C_{\text{V}} = \frac{\mathrm{d}s}{\mathrm{d}\theta}\theta. \tag{3.8}$$

Furthermore, for the application to metals, a constant specific heat capacity (i.e. $C_{\text{V}} = \text{const.}$) is a valid assumption, utilised e.g. in Adam and Ponthot [1], Ghadiani [48], Ibrahimbegovic and Chorfi [61], and Simo and Miehe [122]. Accordingly, the heat capacity is also assumed to be constant (i.e. $C_{\text{V}} = \text{const.}$), since focus in this work is on the application to metals. Thus, the entropy can be written as

$$s(\theta) = C_{\mathrm{V}} \ln\left(\frac{\theta}{\theta_0}\right), \tag{3.9}$$

after integration, where θ_0 and C_{V} denote the constant initial temperature and the constant specific heat, respectively.

Given the constituive relation for the entropy (Equation (3.2)), the Helmholtz free energy per unit reference volume is found to be

$$\psi(\theta) = -C_{\mathrm{V}} \left[(\theta - \theta_0) - \theta \ln\left(\frac{\theta}{\theta_0}\right) \right], \tag{3.10}$$

Subsequently, the time derivative of the entropy is

$$\dot{s}(\theta) = \frac{\partial s}{\partial \theta}\dot{\theta} = -\frac{\partial^2 \psi}{\partial \theta^2}\dot{\theta} = C_{\mathrm{V}} \frac{1}{\theta}\dot{\theta}. \tag{3.11}$$

As previously mentioned, in a purely thermal analysis the deformation is neglected, consequently the material and spatial heat flux coincide, that is $\boldsymbol{Q} \equiv \boldsymbol{q}$, which is also valid for the material and spatial gradient, hence $\nabla_0 \theta \equiv \nabla \theta$. To satisfy the dissipation inequality due to conduction (Equation (**??**)), a constitutive law for the heat flux has to be chosen associating the heat flux $\boldsymbol{q}$ with its dual variable $\boldsymbol{g}$ and the temperature T. Accordingly, so-called Fourier's law, which is linear and isotropic is utilised, which is defined as

$$\boldsymbol{q} = -k\boldsymbol{g}.$$

Herein, the thermal conductivity k is assumed constant and positive that is $k \geq 0$. Thus, heat is conducted in the direction of decreasing temperatures. Apart from Fourier's law, different constitutive laws for the heat flux are available in the literature, as e.g. Duhamel's law of heat conduction (see e.g. Holzapfel [58]) which uses a positive semi-definite second-order tensor k instead of the constant conductivity k. If Duhamel's law is restricted to thermally isotropic behaviour (i.e. no preferred direction), the conductivity tensor reduces to $k = k\boldsymbol{I}$. If a constant heat conductivity $k = \text{const.}$ is assumed, Fourier's law is recovered as a special form of Duhamel's law. Moreover, e.g. in Holzapfel and Simo [59] and Sherief and Abd El-Latief [117], a variable conductivity ($k \neq \text{const}$ is assumed in the context of elastomers). In Bargmann and Steinmann [13] and Bargmann et al. [14], three different constitutive laws for the heat flux $\boldsymbol{q}$ are proposed based on the Green-Naghdi's non-classical theory. Nevertheless, for the present work Fourier's law yields physical results and hence is exclusively considered in this work.

No extra internal variables $\boldsymbol{\alpha}$ are considered in the present description of the thermal problem. Thus, the thermal constitutive initial value problem given the standard assumptions laid out above accepts a closed form solution, i.e., the functions for $\boldsymbol{q}$ and s can be computed directly.

Problem 3.2 | "Standard" thermal constitutive initial value problem.

Given the history of the temperature distribution

$$\theta(t), \quad t \in [t_0, t_{\text{end}}],$$

compute the functions for $\boldsymbol{q}(t)$ and $s(t)$ at every $t \in [t_0, t_{\text{end}}]$ using the constitutive equations

$$s = C_{\text{V}} \ln\left(\frac{\theta}{\theta_0}\right), \tag{3.12}$$

$$\boldsymbol{q} = -k\boldsymbol{g}. \tag{3.13}$$

3.3 Weak energy balance equation

The solution of the thermal problem using the FEM requires the use of the weak form of the energy balance equation. It can be found applying to the governing equation (Equation (3.1)) in the strong form, a variational approach.

Problem 3.3 | Weak energy balance equation

There is energy balance in the body if and only if the temperature distribution satisfies

$$\int_\Omega \left[\left(\dot{e} - \rho r\right)\xi - \boldsymbol{q}\cdot\nabla\xi\right] \mathrm{d}v - \int_{\partial\Omega} \boldsymbol{q}\cdot\boldsymbol{n}_0\xi \,\mathrm{d}a = 0, \quad \forall\boldsymbol{\xi} \in \mathscr{W}, \tag{3.14}$$

where $\mathscr{W}$ is the space of virtual temperature distributions on the body, defined by the space of sufficiently regular arbitrary temperature distributions.

3.4 The thermal initial boundary value problem

Following the same approach as in Section **??**, it is now possible to introduce the the thermal initial boundary value problem. Assume that the internal variables governing the body $\mathscr{B}$ are known at the initial time t_0. In addition, assume that the heat generated in the interior of the body is prescribed, $r(\boldsymbol{x}, t)$, $t \in [t_0, t_{\text{end}}]$, as well as,

- **Natural (or Neumann) boundary condition.** The boundary portion $\partial\Omega_{\text{heat}}$ of $\mathscr{B}$ is subject to a prescribed history of heat flux, $\hat{q}_{\text{presc}}(\boldsymbol{x}, t) = \boldsymbol{q}_{\text{presc}}(\boldsymbol{x}, t)\cdot\boldsymbol{n}(\boldsymbol{x})$, $\boldsymbol{x} \in \partial\Omega_{\text{heat}}$, $t \in [t_0, t_{\text{end}}]$.
- **Essential (or Dirichlet) boundary condition.** The boundary portion $\partial\Omega_{\text{temperature}}$ of $\mathscr{B}$ is subject to a prescribed temperature history, $\theta_{\text{presc}}(\boldsymbol{x}, t)$, $\boldsymbol{x} \in \partial\Omega_{\text{temperature}}$, $t \in [t_0, t_{\text{end}}]$.

As before the admissible temperature distributions for the body $\mathscr{B}$ are all sufficiently regular temperature fields that satisfy the essential boundary condition,

$$\mathscr{K} = \{\theta : \Omega \times \mathbb{R} \to \mathbb{R} \,|\, \theta(\boldsymbol{x}, t) = \theta_{\text{presc}}(\boldsymbol{x}, t), \quad \boldsymbol{x} \in \partial\Omega_{\text{temperature}}, \quad t \in [t_0, t_{\text{end}}]\}. \tag{3.15}$$

Combining the weak energy balance equations with the "standard" thermal constitutive initial value problem the weak form of the "standard" thermal constitutive initial boundary value problem can be stated as follows

Problem 3.4 | "Standard" thermal initial BVP.

Find an admissible temperature distribution, $\theta \in \mathscr{K}$, such that for every $t \in [t_0, t_{\text{end}}]$, the body $\mathscr{B}$ is in energetic equilibrium

$$\int_\Omega \left[\left(C_V \dot{\theta} - \rho r \right) \xi + k \boldsymbol{g} \cdot \nabla \xi \right] \mathrm{d}v - \int_{\partial\Omega} \hat{q} \xi \, \mathrm{d}a = 0, \quad \forall \boldsymbol{\xi} \in \mathscr{W}, \tag{3.16}$$

where the space of virtual temperature distributions at time t is defined by

$$\mathscr{W} \equiv \left\{ \xi : \Omega_0 \to \mathbb{R} \mid \xi = 0 \quad \text{in} \quad \partial\Omega_{\text{temperature},0} \right\}. \tag{3.17}$$

3.5 Finite Element Method

By convenience, the global shape functions can be assembled in the so-called global interpolation matrix as

$$\mathbf{N}^g(\boldsymbol{x}) \equiv \left[N_1^g(\boldsymbol{x}), N_2^g(\boldsymbol{x}), \ldots, N_{n_{\text{points}}}^g(\boldsymbol{x}) \right], \tag{3.18}$$

$$\Theta(t) = \left[\theta^1(t), \ldots, \theta^{n_{\text{points}}}(t) \right]^T. \tag{3.19}$$

$$^h\theta(\boldsymbol{x}, t) \equiv \mathbf{N}^g(\boldsymbol{x}) \Theta(t), \quad ^h\theta \in {}^h\mathscr{K}. \tag{3.20}$$

$$\mathbf{H}^g \equiv \begin{bmatrix} \dfrac{\partial N_1^g}{\partial x} & \dfrac{\partial N_2^g}{\partial x} & \cdots & \dfrac{\partial N_{n_{\text{points}}}^g}{\partial x} \\ \dfrac{\partial N_1^g}{\partial y} & \dfrac{\partial N_2^g}{\partial y} & \cdots & \dfrac{\partial N_{n_{\text{points}}}^g}{\partial y} \end{bmatrix}. \tag{3.21}$$

Problem 3.5 | Material incremental discretized mechanical initial BVP.

Given the initial temperature distribution θ at t_0, the prescribed heat sources and heat fluxes $r(\boldsymbol{x}, t)$ and $\hat{q}(\boldsymbol{x}, t)$ find the admissible nodal temperatures $\theta(t) \in {}^h\mathscr{K}$ such that the body $\mathscr{B}$ is in energetic equilibrium

$$\mathbf{C}\dot{\Theta}(t) + \mathbf{K}\Theta(t) - \mathbf{f}^{\text{ext}}(t) = \mathbf{0}, \tag{3.22}$$

where $\mathbf{C}$ and $\mathbf{K}$ are the temperature damping and stiffness matrix defined as

$$\mathbf{C} = \int_{^h\Omega} C_V \mathbf{N}^{g\,T} \mathbf{N}^g \, \mathrm{d}v., \tag{3.23}$$

$$\mathbf{K} = \int_{^h\Omega} k \mathbf{H}^{g\,T} \mathbf{H}^g \, \mathrm{d}v. \tag{3.24}$$

and $\mathbf{f}^{\text{ext}}(t)$ is the global vector of external forces defined as

$$\mathbf{f}^{\text{ext}}(t) \equiv \int_{h\Omega} \rho \mathbf{N}^{g\,T} r(\boldsymbol{x}, t)\,\mathrm{d}v + \int_{\partial^h \Omega_{\text{heat}}} \mathbf{N}^{g\,T} \hat{q}(\boldsymbol{x}, t)\,\mathrm{d}a. \tag{3.25}$$

Chapter 4

Mechanical problem

In the following chapter, the general framework presented in the previous chapter is applied to a purely mechanical analysis, neglecting the thermal terms.

4.0.1 Mechanical constitutive initial value problem

In the purely mechanical case, with all the quantities related to the thermal domain removed, a constitutive model based on internal variables is established by the following set of equations

$$\boldsymbol{P} = \rho_0 \frac{\partial \psi}{\partial \boldsymbol{F}}, \tag{4.1}$$

$$s = -\frac{\partial \psi}{\partial \theta}, \tag{4.2}$$

$$\psi = \psi(\boldsymbol{F}, \theta, \nabla_0 \theta, \boldsymbol{\alpha}), \tag{4.3}$$

$$\dot{\boldsymbol{\alpha}} = f(\boldsymbol{F}, \theta, \nabla_0 \theta, \boldsymbol{\alpha}), \tag{4.4}$$

$$\frac{1}{\theta} \nabla_0 \theta = g(\boldsymbol{F}, \theta, \boldsymbol{\alpha}). \tag{4.5}$$

Thus, the spatial mechanical constitutive initial value problem can be stated as follows

the single effects. To emphasize this additive decomposition, the Helmholtz free energy ψ in (5.7) is expressed with respect to the reference volume, so that ψ is reformulated using potential functions according to

$$\rho_0 \psi\left(\boldsymbol{F}, T, \operatorname{grad} T, \boldsymbol{\alpha}_{\mathrm{k}}, \boldsymbol{X}\right) := \hat{\mathbb{U}}\left(J^e\right) + \hat{\mathbb{W}}(\tilde{\boldsymbol{F}}) + \hat{\mathbb{M}}\left(J^e, T\right) + \hat{\mathbb{T}}(T) + \hat{\mathbb{K}}\left(\boldsymbol{\alpha}_k, T\right)$$

where in contrast to the deformation gradient $\boldsymbol{F}$, the Jacobi-determinant J^e(5.6) and the isochoric deformation gradient $\tilde{\boldsymbol{F}}$(2.36) are applied. $\hat{U}$ and $\mathbb{W}$ can be identified with the standard hyperelastic materials potentials according to (3.57), whereas $\hat{M}\left(J^e, T\right)$ describes the thermomechanical coupling potential. The potential $\hat{\mathbb{T}}(T)$ represents the purely thermal potential and is assumed identical to (4.8). Finally, $\hat{\mathbb{K}}\left(\boldsymbol{\alpha}_{\mathrm{k}}, T\right)$ is the convex plastic potential. Subsequently, based on the potential functions, the coupling of the two fields structure and thermo can be explained: the temperature enters the structural field via additional thermal stresses and possibly moreover via temperature-dependent material parameters. Herein, $\mathbb{M}\left(J^e, T\right)$ characterizes the thermomechanical coupling potential, leading to thermal stresses and moreover to thermal expansion and dilatation, whereas $\mathbb{K}\left(\boldsymbol{\alpha}_{\mathrm{k}}, T\right)$ being

temperature-dependent and therefore enables exemplarily von Mises plasticity combined with temperature-dependent isotropic hardening and thermal softening. This is in accordance to Agelet de Saracibar et al. [2], Ibrahimbegovic and Chorfi [61], but in contrast to Simo and Miehe [122], who assumed an isothermal plastic potential $\mathbb{K}_{\text{Simo}}\left(\boldsymbol{\alpha}_{\text{k}}\right)$. In contrast, the structure enters the themal field via coupling terms, arising from $\hat{\mathbb{M}}\left(J^e,T\right)$ and $\mathbb{K}\left(\boldsymbol{\alpha}_k,T\right)$, in addition to the purely thermal energy (4.8). Thus, coupling terms as the internal or mechanical dissipation $\mathscr{D}_{\text{mech}}$ may emerge in the thermal balance equation. Furthemore, for finite defomation TSI, where the initial domain Ω_0 deforms to Ω, so that $\Omega \neq \Omega_0$, and a Lagrangian formulation is used, the deformation enters the thermal field additionally due to the mapping of all quantities in the balance equations to the reference configuration.

Likewise, in a material description it can be stated as

Problem 4.1 | Material thermomechanical constitutive initial value problem.

Given the initial values of the internal variables, $\boldsymbol{\alpha}(t_0)$, the history of the deformation gradient

$$\boldsymbol{F}(t), \quad t \in [t_0, t_{\text{end}}], \tag{4.6}$$

and the history of the temperature distribution

$$\theta(t), \quad t \in [t_0, t_{\text{end}}], \tag{4.7}$$

find the functions for $\boldsymbol{P}(t)$, $s(t)$, $\boldsymbol{Q}(t)$ and $\boldsymbol{\alpha}(t)$ such that the constitutive equations

$$\boldsymbol{P} = \rho_0 \frac{\partial \psi}{\partial \boldsymbol{F}}, \tag{4.8}$$

$$s = C_V \ln\left(\frac{\theta}{\theta_0}\right) - \frac{1}{\rho_0}\left(\frac{\partial \hat{\mathbb{M}}\left(J^e,\theta\right)}{\partial \theta} + \frac{\partial \hat{\mathbb{K}}\left(\alpha_k,\theta\right)}{\partial \theta}\right), \tag{4.9}$$

$$\psi = \frac{1}{\rho_0}\left(\hat{\mathbb{U}}\left(J^e\right) + \hat{\mathbb{W}}(\tilde{\boldsymbol{F}}) + \hat{\mathbb{M}}\left(J^e,\theta\right) + \hat{\mathbb{T}}(\theta) + \hat{\mathbb{K}}\left(\boldsymbol{\alpha}_{\text{k}},\theta\right)\right), \tag{4.10}$$

$$\boldsymbol{Q} = -k_0 \boldsymbol{C}^{-1} \nabla_0 \theta, \tag{4.11}$$

$$\dot{\boldsymbol{\alpha}} = f(\boldsymbol{F},\theta,\nabla_0\theta,\boldsymbol{\alpha}), \tag{4.12}$$

are satisfied for every $t \in [t_0, t_{\text{end}}]$, where

$$\hat{\mathbb{T}}(\theta) = -C_{\text{V}}\left[\left(\theta-\theta_0\right) - \theta \ln\left(\frac{\theta}{\theta_0}\right)\right]. \tag{4.13}$$

4.0.2 Weak equilibrium. The principle of virtual work

The strong equations that enforce the equilirium of a body can be writen using the spatial description as

$$\rho \ddot{\boldsymbol{u}} = \operatorname{div}\boldsymbol{\sigma} + \boldsymbol{b} \quad \text{in } \Omega. \tag{4.14}$$

From a practical standpoint, finding the exact solution to the strong equilibrium equations in the context of real engineering problems is most often nearly or entirely impossible. Most numerical methods obtain only approximate solutions to the so-called weak equilibrium equations to circumvent this problem. These result from relaxing the strong equilibrium equations so that the solutions need only satisfy the

equilibrium equations in an average sense instead of satisfying them pointwise. This is achieved through an integration over the body volume. The weak equilibrium equations can be found making use of several energetic and weighted residual methods, such as the Virtual Work Principle used here.

The principle of virtual work can be expressed in a completly equivalent way using a material description.

Problem 4.2 | Weak form of the linear momentum and energy balance equations (material version).

In a material description, the body is in mechanical and energetic equilibrium if and only if the First Piola-Kirchhoff stress field, $\boldsymbol{P}(t)$, the heat flow $\boldsymbol{Q}(t)$, satisfy

$$\int_{\Omega_0} [\boldsymbol{P}(t) : \nabla_0 \boldsymbol{\eta} - (\boldsymbol{b}_0(t) - \rho_0 \ddot{\boldsymbol{u}}(t)) \cdot \boldsymbol{\eta}] \, \mathrm{d}v - \int_{\partial\Omega_0} \boldsymbol{t}_0(t) \cdot \boldsymbol{\eta} \, \mathrm{d}da = 0, \quad \forall \boldsymbol{\eta} \in \mathscr{V}, \tag{4.15}$$

$$\int_{\Omega_0} \left[\rho_0 \left(\dot{e}(t) - r(t) \right) \xi - \boldsymbol{Q}(t) \cdot \nabla_0 \xi \right] \mathrm{d}v - \int_{\partial\Omega_0} \boldsymbol{Q}(t) \cdot \boldsymbol{n}_0 \xi \, \mathrm{d}a = 0, \quad \forall \xi \in \mathscr{W}, \tag{4.16}$$

where $\mathscr{V}$ is the space of virtual displacement of the body, defined by the space of sufficiently regular arbitrary displacements

$$\boldsymbol{\eta} : \Omega \to \mathscr{U}. \tag{4.17}$$

and $\mathscr{W}$ is the space of virtual temperature distributions of the body, defined by the space of sufficiently regular arbitrary temperature distributions

$$\xi : \Omega \to \mathbb{R}. \tag{4.18}$$

4.0.3 Mechanical constitutive initial boundary value problem

It is now possible to pose the mechanical constitutive initial value problem in its weak form. Assume that a body $\mathscr{B}$ is made from a generic material, characterized by a given constitutive model, whose internal variables are known at the initial time, as presented in Figure **??**. In addition, it is assumed that the interior of the body was subjected to a prescribed history of body forces, $\boldsymbol{b}(\boldsymbol{X}, t)$, $t \in [t_0, t_{\text{end}}]$, and to the following boundary conditions:

- **Natural (or Neumann) boundary condition:** The boundary portion $\Omega_{\text{traction, 0}}$ of $\mathscr{B}$ is subjected to a prescribed history of traction forces, $\boldsymbol{t}_{\text{presc}}(\boldsymbol{X}, t)$, $\boldsymbol{X} \in \partial\Omega_{\text{traction},0}$, $t \in [t_0, t_{\text{end}}]$,

- **Essential (or Dirichlet) boundary condition:** The boundary portion $\Omega_{\text{motion, 0}}$ of $\mathscr{B}$ is subjected to a prescribed displacement field history, $\boldsymbol{u}_{\text{presc}}(\boldsymbol{X}, t)$, such that

$$\boldsymbol{\varphi}(\boldsymbol{X}, t) = \boldsymbol{X} + \boldsymbol{u}_{\text{presc}}(\boldsymbol{X}, t), \quad \boldsymbol{X} \in \partial\Omega_{\text{motion, 0}}, \quad t \in [t_0, t_{\text{end}}].$$

It is also convenient to define the set of kinematically admissible displacements of $\mathscr{B}$ as the set of all sufficiently regular displacement functions tha satisfy the essential boundary condition (**?**),

$$\mathscr{K} \equiv \{\boldsymbol{u} : \Omega \times \mathscr{R} \to \mathscr{U} \mid \boldsymbol{u}(\boldsymbol{X}, t) = \boldsymbol{u}_{\text{presc}}(\boldsymbol{X}, t), \quad \boldsymbol{X} \in \partial\Omega_{\text{motion},0}, \quad t \in [t_0, t_{\text{end}}]\}. \tag{4.19}$$

$$\dot{e} \equiv \dot{\psi} + s\dot{\theta} + \dot{s}\theta. \tag{4.20}$$

$$\dot{s}\left(\boldsymbol{F}, \theta, \boldsymbol{\alpha}_{\text{k}}\right) = \text{C}_{\text{V}} \frac{1}{\theta}\dot{\theta} - \frac{1}{\theta}\mathcal{H}^{\text{ep}} \tag{4.21}$$

$$\mathcal{H}^{\text{ep}} = \frac{\theta}{\rho_0}\left(\frac{\partial^2 \hat{\text{M}}\left(J^e, T\right)}{\partial T \partial J^e} j^e + \frac{\partial^2 \hat{\text{M}}\left(J^e, T\right)}{\partial T^2}\dot{T} + + \frac{\partial^2 \hat{\mathbb{K}}\left(\boldsymbol{\alpha}_k, T\right)}{\partial T^2}\dot{T} + \frac{\partial^2 \hat{\mathbb{K}}\left(\boldsymbol{\alpha}_k, T\right)}{\partial T \partial \boldsymbol{\alpha}_k} \star \dot{\alpha}_k\right) \tag{4.22}$$

So the weak form of the quasi-static mechanical constitutive initial boundary value problem can be stated in a spatial description as follows and in the material description as

Problem 4.3 | Material mechanical initial BVP.

Find a kinematically admissible displacement function, $\boldsymbol{u} \in \mathscr{K}_u$, and an admissible temperature distribution, $\theta \in \mathscr{K}_\theta$, such that for every $t \in [t_0, t_{\text{end}}]$, the body $\mathscr{B}$ is in mechanical and energetic equilibrium

$$\int_{\Omega_0} [\boldsymbol{P}(t) : \nabla_0 \boldsymbol{\eta} - (\boldsymbol{b}_0(t) - \rho_0 \ddot{\boldsymbol{u}}(t)) \cdot \boldsymbol{\eta}] \, \mathrm{d}v - \int_{\partial\Omega_0} \boldsymbol{t}_0(t) \cdot \boldsymbol{\eta} \, \mathrm{d}a = 0, \quad \forall \boldsymbol{\eta} \in \mathscr{V}, \tag{4.23}$$

$$\int_{\Omega_0} \left[\left(\rho_0 C_{\text{V}} \dot{\theta}(t) - \mathscr{D}_{\text{mech}}(t) - \mathcal{H}^{\text{ep}}(t) - \rho_0 r(t)\right)\xi - \boldsymbol{Q}(t) \cdot \nabla_0 \xi\right] \mathrm{d}v - \int_{\partial\Omega_0} \boldsymbol{Q}(t) \cdot \boldsymbol{n}_0 \xi \, \mathrm{d}a = 0, \quad \forall \xi \in \mathscr{W}, \tag{4.24}$$

where the space of virtual displacements at time t is defined by

$$\mathscr{V} \equiv \left\{\boldsymbol{\eta} : \Omega_0 \to \mathscr{U} \mid \boldsymbol{\eta} = \boldsymbol{0} \quad \text{in} \quad \partial\Omega_{\text{motion},0}\right\}, \tag{4.25}$$

and at each point of $\mathscr{B}$, the First Piola-Kirchhoff stress tensor is the solution of material mechanical constitutive initial values problem.

4.1 Time descretization

In the context of thermo-mechanical problems, a generic path-dependent model is a model in which the thermodynamical state does not depend only on the instantaneous deformation and temperature states but also on their history. Under these conditions, the solution of the constitutive initial value problem for a given set of initial conditions is usually not known for complex strain, $\boldsymbol{F}(t)$, or temperature paths, $\theta(t)$, paths. Thus, as in the domain of a stricly mechanical problem, there is a need to use an appropriate numerical algorithm to integrate the rate constitutive equations.

Attending to the thermo-mechanical constitutive initial boundary value problem and considering the time increment $[t_n, t_{n+1}]$, this approach is comprised by the following requirements:

- **First Piola-Kirchhoff stress tensors.** Considering a time increment $[t_n, t_{n+1}]$ and given the set $\boldsymbol{\alpha}_n$ of internal variables at t_n, the deformation gradient $\boldsymbol{F}_{n+1}$ and the temperature distribution θ_{n+1} at time t_{n+1} determines the First Piola-Kirchhoff stress tensor $\boldsymbol{P}_{n+1}$ uniquely as

$$\boldsymbol{P}_{n+1} = \hat{\boldsymbol{P}}(\boldsymbol{F}_{n+1}, \theta_{n+1}, \boldsymbol{\alpha}_n), \tag{4.26}$$

  where $\hat{\boldsymbol{P}}$ is the incremental constitutive function for the First Piola-Kirchhoff stress tensor.

- **Set of internal variables.** Assuming that the set of internal variables $\boldsymbol{\alpha}_n$ is known at t_n, the set of internal variables must be uniquely determined by the prescribed deformation gradient $\boldsymbol{F}_{n+1}$ and temperature distribution θ_{n+1} prescribed at t_{n+1} as

$$\boldsymbol{\alpha}_{n+1} = \hat{\boldsymbol{\alpha}}(\boldsymbol{F}_{n+1}, \theta_{n+1}, \boldsymbol{\alpha}_n), \tag{4.27}$$

  where $\hat{\boldsymbol{\alpha}}$ is the incremental constitutive function for the set of internal variables.

- **Mechanical dissipation.** Considering a time increment $[t_n, t_{n+1}]$ and given the set $\boldsymbol{\alpha}_n$ of internal variables at t_n, the deformation gradient $\boldsymbol{F}_{n+1}$ and the temperature distribution θ_{n+1} at time t_{n+1} determines the mechanical dissipation $\mathcal{D}_{\text{mech}}$ as

$$\mathcal{D}_{\text{mech},n+1} = \hat{\mathcal{D}}_{\text{mech}}(\boldsymbol{F}_{n+1}, \theta_{n+1}, \boldsymbol{\alpha}_n). \tag{4.28}$$

- **Gough-Joule effect.** Considering a time increment $[t_n, t_{n+1}]$ and given the set $\boldsymbol{\alpha}_n$ of internal variables at t_n, the deformation gradient $\boldsymbol{F}_{n+1}$ and the temperature distribution θ_{n+1} at time t_{n+1} determines the Gough-Joule effect $\mathcal{H}^{\text{ep}}$ as

$$\mathcal{H}^{\text{ep}}_{n+1} = \hat{\mathcal{H}}^{\text{ep}}(\boldsymbol{F}_{n+1}, \theta_{n+1}, \boldsymbol{\alpha}_n). \tag{4.29}$$

Generally, the numerical constitutive laws are nonlinear and path-independent within one increment.

Making use of the aforementioned time discretization, one can state the weak form of the mechanical constffitutive initial boundary value problem in the spatial description as and in the material description as

Problem 4.4 | Material incremental thermo-mechanical initial BVP.

Given the set of internal variables $\boldsymbol{\alpha}_n$ at t_n, the prescribed body and traction force fields $\boldsymbol{b}_{0,n+1}$ and $\boldsymbol{t}_{0,n+1}$, as well as, the prescribed heat sources, $\boldsymbol{r}_{n+1}$ and

heat fluxes, $h_{0,n+1}$, at t_{n+1}, and the prescribed deformation gradient $\boldsymbol{F}_{n+1}$ and temperature distribution θ_{n+1} at t_{n+1}, find the kinematically admissible displacement field $\boldsymbol{u}_{n+1} \in \mathscr{K}_{u,n+1}$ and the admissible temperature distribution $\theta_{n+1} \in \mathscr{K}_{\theta,n+1}$ such that the body $\mathscr{B}$ is in mechanical and energetic equilibrium

$$f \int_{\Omega_{n+1}} [\hat{\boldsymbol{P}}(\boldsymbol{F}(\boldsymbol{u}_{n+1}), \theta_{n+1}, \boldsymbol{\alpha}_n) : \nabla_0 \boldsymbol{\eta} - (\boldsymbol{b}_{0,n+1} - \rho_0 \ddot{\boldsymbol{u}}_{n+1}) \cdot \boldsymbol{\eta}] \, \mathrm{d}v - \int_{\partial\Omega_{n+1}} \boldsymbol{t}_{0,n+1} \cdot \boldsymbol{\eta} \, \mathrm{d}a = 0, \quad \forall \boldsymbol{\eta} \in \mathscr{V}_{u,n+1}, \tag{4.30}$$

$$\int_{\Omega_0} \left[\left(\rho_0 C_V \dot{\theta}_{n+1} - \hat{\mathcal{D}}_{\mathrm{mech}}(\boldsymbol{F}(\boldsymbol{u}_{n+1}), \theta_{n+1}, \boldsymbol{\alpha}_n) - \hat{\mathcal{H}}^{\mathrm{ep}}(\boldsymbol{F}(\boldsymbol{u}_{n+1}), \theta_{n+1}, \boldsymbol{\alpha}_n) - \rho_0 r_{n+1} \right) \xi - \boldsymbol{Q}_{n+1} \cdot \nabla_0 \xi \right] \mathrm{d}v - \int_{\partial\Omega_0} \hat{Q}_{n+1} \xi \, \mathrm{d}a = 0, \quad \forall \xi \in \mathscr{V}_{\theta,n+1}, \tag{4.31}$$

where

$$\mathscr{K}_{u,n+1} \equiv \{ \boldsymbol{u} : \Omega \times \mathscr{R} \to \mathscr{U} \mid \boldsymbol{u}_{n+1}(\boldsymbol{X}) = \boldsymbol{u}_{\mathrm{presc},n+1}(\boldsymbol{X}),\ \boldsymbol{X} \in \partial\Omega_{\mathrm{motion},0} \}, \tag{4.32}$$

$$\mathscr{K}_{\theta,n+1} \equiv \{ \boldsymbol{u} : \Omega \times \mathscr{R} \to \mathscr{R} \mid \theta_{n+1}(\boldsymbol{X}) = \theta_{\mathrm{presc},n+1}(\boldsymbol{X}),\ \boldsymbol{X} \in \partial\Omega_{\mathrm{temperature},0} \}. \tag{4.33}$$

4.2 Finite Element Method

It is now possible to apply the finite element method to discretize spatial the incremental thermo-mechanical initial boundary value problem. The approach is entirely similar to the one present in the context of the strictly mechancial (see Section **??**) and stricly thermal (see Section **??**) problems. As such some details are ommited.

Defining the global vector of nodal displacements as

$$\mathbf{u} = \left[u_1^1, \ldots, u_{n_{\mathrm{dim}}}^1, \ldots, u_1^{n_{\mathrm{points}}}, \ldots, u_{n_{\mathrm{dim}}}^{n_{\mathrm{points}}} \right]^T, \tag{4.34}$$

the displacement field $\vec{u}(\boldsymbol{x})$m defined over the global domain Ω, can be found from Equation (2.31) at any point $\boldsymbol{x}$ as

The global shape functions can be conveniently assembled in the so-called global interpolation matrix as

$$\mathbf{N}^g(\boldsymbol{x}) \equiv \left[\mathrm{diag}[N_1^g(\boldsymbol{x})] \ \mathrm{diag}[N_2^g(\boldsymbol{x})] \ \cdots \ \mathrm{diag}[N_{n_{\mathrm{points}}}^g(\boldsymbol{x})] \right], \tag{4.35}$$

where $\mathrm{diag}[N_i^g]$ is a diagonal matriz $n_{\mathrm{dim}} \times n_{\mathrm{dim}}$

$$\mathrm{diag}[N_i^g(\boldsymbol{x})] \equiv \begin{bmatrix} N_i^g & 0 & \cdots & 0 \\ 0 & N_i^g & \cdots & 0 \\ \vdots & \vdots & \ddots & \vdots \\ 0 & 0 & \cdots & N_i^g \end{bmatrix} \tag{4.36}$$

where n_{dim} is the number of degrees of freedom per node.

$$ {}^h\boldsymbol{u}(\boldsymbol{x}) \equiv \mathbf{N}^{g,u}(\boldsymbol{x})\mathbf{u}, \quad {}^h\boldsymbol{u} \in {}^h\mathscr{K}, \tag{4.37} $$

$$ {}^h\theta(\boldsymbol{x}) \equiv \mathbf{N}^{g,\theta}(\boldsymbol{x})\theta, \quad {}^h\boldsymbol{\theta} \in {}^h\mathscr{K}_\theta. \tag{4.38} $$

4.2.1 Spatial discretization

Applying the aforementioned finite element discretization to the incremental mechanical constitutive initial boundary value problem, we can then write in the spatial description

$$ \int_{{}^h\Omega} \left[\hat{\boldsymbol{\sigma}}^T \mathbf{B}^g \boldsymbol{\eta} - (\mathbf{b}_{n+1} - \rho\ddot{\mathbf{u}}_{n+1}) \cdot \mathbf{N}^g \boldsymbol{\eta} \right] \mathrm{d}v - \int_{\partial^h\Omega_{\text{traction}}} \mathbf{t}_{n+1} \cdot \mathbf{N}^g \boldsymbol{\eta} \, \mathrm{d}a = 0, \quad \forall \boldsymbol{\eta} \in {}^h\mathscr{V}, \tag{4.39} $$

where $\mathbf{B}^g$ is the discrete symmetric global gradient operator, defined for a 2D problem in cartesian coordinates as

$$ \mathbf{B}^g \equiv \begin{bmatrix} \frac{\partial N_1^g}{\partial x} & 0 & \frac{\partial N_2^g}{\partial x} & 0 & \cdots & \frac{\partial N_{n_{\text{points}}}^g}{\partial x} & 0 \\ 0 & \frac{\partial N_1^g}{\partial y} & 0 & \frac{\partial N_2^g}{\partial y} & \cdots & 0 & \frac{\partial N_{n_{\text{points}}}^g}{\partial y} \\ \frac{\partial N_1^g}{\partial y} & \frac{\partial N_1^g}{\partial x} & \frac{\partial N_2^g}{\partial y} & \frac{\partial N_2^g}{\partial x} & \cdots & \frac{\partial N_{n_{\text{points}}}^g}{\partial y} & \frac{\partial N_{n_{\text{points}}}^g}{\partial x} \end{bmatrix}. \tag{4.40} $$

Equation (4.39) can be rewritten as

$$ \left\{ \int_{{}^h\Omega} \left[\mathbf{B}^{g\,T} \hat{\boldsymbol{\sigma}}(\boldsymbol{\alpha}_n, \boldsymbol{F}_{n+1}) - \mathbf{N}^{g\,T} \mathbf{b}_{n+1} + \mathbf{N}^{g\,T} \rho\ddot{\mathbf{u}}_{n+1} \right] \mathrm{d}v - \int_{\partial^h\Omega_{\text{traction}}} \mathbf{N}^{g\,T} \mathbf{t}_{n+1} \, \mathrm{d}a \right\}^T \boldsymbol{\eta} = 0, \quad \forall \boldsymbol{\eta} \in {}^h\mathscr{V}, \tag{4.41} $$

and, since it must be satisfied for any $\boldsymbol{\eta} \in {}^h\mathscr{V}$, the incremental quasi-static discretized mechanical constitutive initial boundary value problem can thus be stated in the spatial description as

In a material description, Equation (4.41) is written as

$$ \left\{ \int_{{}^h\Omega_0} \left[\mathbf{G}^{g\,T} \hat{\boldsymbol{P}}(\boldsymbol{\alpha}_n, \boldsymbol{F}_{n+1}) - \mathbf{N}^{g\,T} \mathbf{b}_{0,n+1} + \mathbf{N}^{g\,T} \rho_0\ddot{\mathbf{u}}_{n+1} \right] \mathrm{d}v - \int_{\partial^h\Omega_{\text{traction},0}} \mathbf{N}^{g\,T} \mathbf{t}_{0,n+1} \, \mathrm{d}a \right\}^T \boldsymbol{\eta} = 0, \quad \forall \boldsymbol{\eta} \in {}^h\mathscr{V}, \tag{4.42} $$

where $\mathbf{G}^g$ is the discrete global gradient operator, defined for a 2D problem in cartesian

coordinates as

$$\mathbf{G}^g \equiv \begin{bmatrix} \frac{\partial N_1^g}{\partial x} & 0 & \frac{\partial N_2^g}{\partial x} & 0 & \cdots & \frac{\partial N_{n_{\text{points}}}^g}{\partial x} & 0 \\ 0 & \frac{\partial N_1^g}{\partial x} & 0 & \frac{\partial N_2^g}{\partial x} & 0 & \cdots & \frac{\partial N_{n_{\text{points}}}^g}{\partial x} \\ \frac{\partial N_1^g}{\partial y} & 0 & \frac{\partial N_2^g}{\partial y} & \cdots & 0 & \frac{\partial N_{n_{\text{points}}}^g}{\partial y} & 0 \\ 0 & \frac{\partial N_1^g}{\partial y} & 0 & \frac{\partial N_2^g}{\partial y} & \cdots & 0 & \frac{\partial N_{n_{\text{points}}}^g}{\partial y} \end{bmatrix}, \tag{4.43}$$

and, as for the spatial description, it must be satisfied for any $\boldsymbol{\eta} \in {}^h\mathscr{V}$, the incremental quasi-static discretized mechanical constitutive initial boundary value problem can thus be stated in the material description as

Problem 4.5 | Material incremental discretized mechanical initial BVP.

Given the set of internal variables $\boldsymbol{\alpha}_n$ at t_n, the prescribed body and traction force fields $\boldsymbol{b}_{0,n+1}$ and $\boldsymbol{t}_{0,n+1}$, and the prescribed deformation gradient $\boldsymbol{F}_{n+1}$ at t_{n+1}, find the kinematically admissible nodal displacement field $\boldsymbol{u}_{n+1} \in {}^h\mathscr{K}_{n+1}$ such that the body $\mathscr{B}$ is in equilibrium as stated by the Virtual Work Principle

$$\mathbf{M}\ddot{\mathbf{u}}_{n+1} + \mathbf{f}_u^{\text{int}}(\Theta_{n+1}, \mathbf{u}_{n+1}) - \mathbf{f}_{u,n+1}^{\text{ext}} = \mathbf{0}, \tag{4.44}$$

$$\mathbf{C}\ddot{\Theta}_{n+1} + \mathbf{f}_\theta^{\text{int}}(\Theta_{n+1}, \mathbf{u}_{n+1}) - \mathbf{f}_{\theta,n+1}^{\text{ext}} = \mathbf{0}, \tag{4.45}$$

where $\mathbf{f}_u^{\text{int}}$ e $\mathbf{f}_{u,n+1}^{\text{ext}}$ are the global vectors of internal and external forces defined as

$$\mathbf{f}_u^{\text{int}} \equiv \int_{{}^h\Omega_0} \mathbf{G}^{g\,T} \hat{\boldsymbol{P}}(\boldsymbol{F}(\boldsymbol{u}_{n+1}), \theta_{n+1}\boldsymbol{\alpha}_n)\,\mathrm{d}v, \tag{4.46}$$

$$\mathbf{f}_{u,n+1}^{\text{ext}} \equiv \int_{{}^h\Omega_0} \mathbf{N}^{g\,T}\mathbf{b}_{0,n+1}\,\mathrm{d}v + \int_{\partial^h\Omega_{\text{traction},0}} \mathbf{N}^{g\,T}\mathbf{t}_{0,n+1}\,\mathrm{d}a, \tag{4.47}$$

$$\mathbf{f}_\theta^{\text{int}} \equiv \int_{{}^h\Omega_0} \mathbf{N}^{g\,T}\hat{\mathscr{D}}_{\text{mech}}(\boldsymbol{F}(\boldsymbol{u}_{n+1}), \theta_{n+1}\boldsymbol{\alpha}_n) + \hat{\mathcal{H}}^{\text{ep}}(\boldsymbol{F}(\boldsymbol{u}_{n+1}), \theta_{n+1}\boldsymbol{\alpha}_n)\,\mathrm{d}v, \tag{4.48}$$

$$\mathbf{f}_{\theta,n+1}^{\text{ext}} \equiv \int_{{}^h\Omega_0} \mathbf{N}^{g\,T}\mathbf{r}_{0,n+1}\,\mathrm{d}v + \int_{\partial^h\Omega_{\text{heat},0}} \mathbf{N}^{g\,T}\hat{Q}_{n+1}\,\mathrm{d}a. \tag{4.49}$$

and $\mathbf{M}$ is the mass matrix defined as

$$\mathbf{M} = \int_{{}^h\Omega_0} \rho_0 \mathbf{N}^{g\,T}\mathbf{N}^g\,\mathrm{d}v, \mathbf{C} = \int_{{}^h\Omega_0} \rho_0 C_{\text{V}} \mathbf{N}^{g\,T}\mathbf{N}^g\,\mathrm{d}v. \tag{4.50}$$

$$\begin{aligned} \mathcal{H}^e &= \theta m_0 \operatorname{tr}\dot{\varepsilon}^e \\ \mathscr{D}_{\text{mech}} &= \eta : \dot{\varepsilon}^p - \kappa\left(\varepsilon^p\right)\dot{\xi}^p \end{aligned} \tag{4.51}$$

The global vectors for the internal and external forces are usually obtained by

assemblage of their elemental counterparts as

$$\mathbf{f}^{\text{int}} = \mathop{\mathsf{A}}_{e=1}^{n_{\text{elem}}} \left(\mathbf{f}^{\text{int}}\right)^{(e)}, \tag{4.52}$$

$$\mathbf{f}^{\text{ext}} = \mathop{\mathsf{A}}_{e=1}^{n_{\text{elem}}} \left(\mathbf{f}^{\text{ext}}\right)^{(e)}, \tag{4.53}$$

where the elemental vectors in the spatial description are defined as

$$\left(\mathbf{f}^{\text{int}}\right)^{(e)} \equiv \int_{{}^h\Omega^{(e)}} \mathbf{B}^T \hat{\boldsymbol{\sigma}}(\boldsymbol{F}_{n+1}, \boldsymbol{\alpha}_n)\, \mathrm{d}v, \tag{4.54}$$

$$\left(\mathbf{f}^{\text{ext}}_{n+1}\right)^{(e)} \equiv \int_{{}^h\Omega^{(e)}} \mathbf{N}^T \mathbf{b}_{n+1}\, \mathrm{d}v + \int_{\partial {}^h\Omega^{(e)}_{\text{traction}}} \mathbf{N}^T \mathbf{t}_{n+1}\, \mathrm{d}a, \tag{4.55}$$

and in material description as

$$\left(\mathbf{f}^{\text{int}}\right)^{(e)} \equiv \int_{{}^h\Omega_0^{(e)}} \mathbf{G}^T \hat{\boldsymbol{P}}(\boldsymbol{F}_{n+1}, \boldsymbol{\alpha}_n)\, \mathrm{d}v, \tag{4.56}$$

$$\left(\mathbf{f}^{\text{ext}}_{n+1}\right)^{(e)} \equiv \int_{{}^h\Omega_0^{(e)}} \mathbf{N}^T \mathbf{b}_{0,n+1}\, \mathrm{d}v + \int_{\partial {}^h\Omega^{(e)}_{0,\text{ traction}}} \mathbf{N}^T \mathbf{t}_{0,n+1}\, \mathrm{d}a, \tag{4.57}$$

The matrices **N**, **B**, and **G** are the elemental interpolation matrix, the symmetric elemental gradient operator, and the discrete elemental gradient operator.

In a similar manner, the global mass matrix is also usually obtained by assemblage of their elemental counterparts as

$$\mathbf{M} \equiv \mathop{\mathsf{A}}_{e=1}^{n_{\text{elem}}} \mathbf{M}^{(e)}, \tag{4.58}$$

where the elemental mass matrices in the spatial description are defined as

$$\mathbf{M}^{(e)} = \int_{{}^h\Omega^{(e)}} \rho \mathbf{N}^T\, \mathrm{d}v, \tag{4.59}$$

and the material descriptrion

$$\mathbf{M}^{(e)} = \int_{{}^h\Omega_0^{(e)}} \rho_0 \mathbf{N}^T\, \mathrm{d}v. \tag{4.60}$$

4.2.2 Numerical integration

In the Finite Element Method, the integrations over the element domain are generally performed numerically using the Gaussian Quadrature Method. Stating it's application succinctly, let $a(\boldsymbol{x})$ be a generic field, if there is a coordinate transformation from a local (or natural) normalized domain Υ to the element domain $\Omega^{(e)}$, $\boldsymbol{x}\colon \Upsilon \to \Omega^{(e)}$, the integral of $a(\boldsymbol{x})$ over the domain $\Omega^{(e)}$ can be numerically determined as

$$\int_{\Omega^{(e)}} a(\boldsymbol{x})\, \mathrm{d}\boldsymbol{x} = \int_{\Upsilon} a(\boldsymbol{x}(\boldsymbol{\zeta}))\, j(\boldsymbol{\zeta})\, \mathrm{d}\boldsymbol{\zeta} \approx \sum_{i=1}^{n_{\text{GP}}} w_i\, a(\boldsymbol{x}(\boldsymbol{\zeta}_i))\, j(\boldsymbol{\zeta}_i), \tag{4.61}$$

where $\boldsymbol{\zeta}_i$ and w_i, $i = 1,\dots,n_{\text{GP}}$ are the positions and weigths of the Gauss sampling points in the domain Υ and $j(\boldsymbol{\zeta})$ is the determinant of the coordinate trasnformation's Jacobian defined as

$$j(\boldsymbol{\zeta}) = \det\left(\frac{\partial \boldsymbol{x}}{\partial \boldsymbol{\zeta}}\right). \tag{4.62}$$

4.3 Linearisation

The equilibrium equation, Equation (2.41) in a spatial description and Equation (3.22) in a material description, is generally nonlinear due to geometrical and/or material nonlinearities. The Newton-Raphson Method is an efficient and robust iterative scheme with a quadratic convergence rate often used to solve the equilibrium equation at each time increment, t_n. The residual of the fully discretized balance of linear momentum is defined for an iteration step i of the Newton-Raphson method as

$$\mathbf{r}(\mathbf{u}^i_{n+1}) = \mathbf{M}\ddot{\mathbf{u}}^i_{n+1} + \mathbf{f}^{\text{int}}(\mathbf{u}^i_{n+1}) - \mathbf{f}^{\text{ext}}_{n+1}. \tag{4.63}$$

A Taylor expansion about the current solution $\mathbf{u}^i_{n+1}$ is performed, discarding all terms of higher order than one, yielding the linearised form

$$\text{Lin}\,\mathbf{r}(\mathbf{u}^i_{n+1}) = \mathbf{r}(\mathbf{u}^i_{n+1}) + \underbrace{\left.\frac{\partial \mathbf{r}(\mathbf{u}_{n+1})}{\partial \mathbf{u}_{n+1}}\right|^i}_{\mathbf{K}(\mathbf{u}^i_{n+1})} \delta\mathbf{u}. \tag{4.64}$$

with the dynamic effective tangential stiffness matrix $\mathbf{K}(\mathbf{u}^i_{n+1})$. The linearisation of the internal forces included in $\mathbf{K}$ is known as the tangential stiffness matrix $\mathbf{K}_T$, which is defined as

$$\mathbf{K}^i_T = \left.\frac{\partial \mathbf{f}^{\text{int}}}{\partial \mathbf{u}_{n+1}}\right|^i. \tag{4.65}$$

Equilibrium is achieved if

$$\text{Lin}\,\mathbf{r}(\mathbf{u}^i_{n+1}) = \mathbf{0}, \tag{4.66}$$

so that a linear system of equation is given by

$$\mathbf{K}(\mathbf{u}^i_{n+1})\delta\mathbf{u} = -\mathbf{r}\left(\mathbf{u}^i_{n+1}\right). \tag{4.67}$$

Thus, a new solution of the displacement increment $\delta\mathbf{u}$ for current iteration step $i+1$ is determined, and the final displacement solution of time step $n+1$ is obtained via updating

$$\mathbf{u}^{i+1}_{n+1} = \mathbf{u}^i_{n+1} + \delta\mathbf{u}. \tag{4.68}$$

A solution of t_{n+1} is found, i.e. an equilibrium state is reached and $\mathbf{u}_{n+1} = \mathbf{u}^{i+1}_{n+1}$, if prescribed, user-defined convergence criteria are fulfilled.

Correção do TPC de DT

Chapter 5

Solution procedures for coupled fields

This chapter presents an overview of solution procedures for coupled fields. It includes techniques applied to various coupled field problems, such as thermomechanical coupling, fluid-structure interaction, and aeroelasticity. Its goal is to support the choice of solution techniques for thermo-plastic problems, which are accurate, stable, efficient, both in terms of memory and computational time, and easy to implement and extend later to further couplings, e.g., electro-thermomechanical problems.

5.1 Context field elimination

Field elimination achieves the solution of a coupled problem by eliminating the variables of the first field and introducing them into the second field. This second field is then solved.

The main advantage of this procedure is the reduction of the number of state variables. Which in turn, leads to smaller systems of equations, which are presumably easier to solve. Furthermore, the analyst can choose the remaining variables such that they are the variables of interest. In this way, the variables eliminated do not need to be recovered. (Felippa and Park, 1980)

On the other hand Felippa and Park (1980) cite as disadvantages

- only possible for problems allowing explicit (and well-conditioned) variable eliminations;
- sparseness and symmetry attributes of matrices associated with the original coupled system can be adversely affected by the eliminations process; and
- available software modules for the isolated fields are not likely to be of much use for processing the reduced system.

The remainder of the chapter disregards these procedures, including in Section **??** where the comparison of the different schemes is discussed.

5.2 Monolithic

Monolithic algorithms solve the coupled nonlinear multi-physics system simultaneously. Predominantly, implicit schemes are applied to achieve good stability properties. In turn, the nonlinear residual equations are often solved using the Newton-Raphson method. A particular challenge for monolithic algorithms is the efficient solution of the large system of equations, including potential nonlinearities or lack of symmetry. Even the units chosen can contribute to the ill-conditioning of the system matrix. One essential aspect for efficient solvers for large-scale problems is a good preconditioning technique.

5.2.1 Numerical considerations

For the solution of a large system of equations, iterative methods are preferable to direct methods, in part, due to memory footprint considerations. The Newton-Krylov methods such as GMRES and the BiCGStab are among the most commonly used in multi-physics problems (Hron and Turek, 2006). However, their use does not suffice for an efficient and robust solution procedure for a multi-physics problem. In addition, the use of preconditioners alleviates the possible large condition numbers of the system matrix. There are several preconditioning techniques for the solution of large systems of equations, e.g., ILU preconditioners, domain decomposition, including multigrid approaches; multilevel recursive Schur complements preconditioners (see Smith et al. (2004) and Chen (2005)).

Heil (2004) is concerned with the fully coupled solution of large-displacement fluid-structure interaction problems by Newton's method. They use block-triangular approximations of the Jacobian matrix, obtained by neglecting selected fluid-structure interaction blocks, and show that they provide suitable preconditioners for the solution of the linear systems with GMRES. A Schur complement approximation for the Navier-Stokes block and multigrid approximations for the solution of the computationally most expensive operations is the basis for the efficient approximate implementation of the preconditioners.

Hron and Turek (2006) propose a method based on a fully implicit, monolithic formulation of the problem in the arbitrary Lagrangian-Eulerian framework to solve the problem of fluid-structure interaction of an incompressible elastic object in laminar incompressible viscous flow They utilize the standard geometric multigrid approach based on a hierarchy of grids obtained by successive regular refinement of a given coarse mesh. The complete multigrid iteration is performed in the standard defect-correction setup with the V or F-type cycle.

Tezduyar et al. (2006) show how preconditioning techniques more sophisticated than diagonal preconditioning can be used in iterative solutions of the linear equation systems in fluid-structure interaction problems.

In Gee et al. (2011), the authors focus on the strong coupling fluid-structure interaction employing monolithic solution schemes. Therein, a Newton-Krylov method is applied to the monolithic set of nonlinear equations. They propose two preconditioners that apply algebraic multigrid techniques to the entire fluid-structure interaction system of equations. As the first option, the authors employ a standard block Gauss-Seidel approach, where approximate inverses of the individual field blocks are based on an algebraic multigrid hierarchy tailored for the type of the underlying physical problem. A monolithic coarsening scheme for the coupled system that uses prolongation and restriction projections constructed for the individual fields

provides the basis for the second preconditioner. The resulting nonsymmetric monolithic algebraic multigrid method involves coupling the fields on coarse approximations to the problem yielding significantly enhanced performance, claim the authors.

In the context of multi-physics problems, Lin et al. (2010) propose a fully coupled algebraic multilevel preconditioner for Newton-Krylov solution methods. A set of multi-physics partial differential equation (PDE) applications attests its performance: a drift-diffusion approximation for semiconductor devices, a low Mach number formulation for the simulation of coupled flow, transport, and non-equilibrium chemical reactions, a low Mach number formulation for visco-resistive magnetohydrodynamics (MHD) systems. An aggressive-coarsening graph-partitioning of the non-zero block structure of the Jacobian matrix provides the basis for the algebraic multilevel preconditioner. Using a different approach Badia et al. (2014) employ a new family of recursive block LU preconditioners to solve the thermally coupled induction less magnetohydrodynamics problem equations, which model the flow of an electrically charged fluid under the influence of an external electromagnetic field with thermal coupling.

Netz (2013) addresses a thermo-mechanically coupled problem of thermo-viscoelasticity at finite strains using a monolithic approach. The authors solve the system of nonlinear algebraic equations obtained from the spatial (FEM) and temporal (diagonally-implicit Runge-Kutta methods) discretization of the problem monolithically. They employ the Multilevel-Newton algorithm to obtain a high-order result in the space and the time domain. The numerical concept is applied to a constitutive model of finite strain thermo-viscoelasticity. Rothe et al. (2015) also employ in the context of thermo-viscoelasticity, the multilevel Newton algorithm to solve the system of algebraic equations describing the discretized problem.

Danowski et al. (2013) presents a monolithic solution scheme for thermo-structure interaction problem, using right preconditioning and a GMRES. The preconditioner "sub-problem" is solved using a Richardson iteration scheme and a relaxed block Gauss-Seidel method, which uncouples the mechanical and thermal problems. This procedure tackles each problem using an independent algebraic multigrid (AMG) preconditioner. Verdugo and Wall (2016) also considers the procedure just mentioned, as well as a preconditioner based on a semi-implicit method for pressure-linked equations, extended to deal with an arbitrary number of fields. This technique also results in uncoupled problems that can be solved with standard AMG. They also introduce a more sophisticated preconditioner that enforces the coupling at all AMG levels, unlike the other two techniques, which resolve the coupling only at the finest level. These techniques are applied successfully to three different coupled problems: thermo-structure interaction, fluid-structure interaction, and a complex model of the human lung.

Mayr et al. (2020) propose a hybrid interface preconditioner for the monolithic solution of surface-coupled problems. They combine physics-based block preconditioners with an additional additive Schwarz preconditioner, whose subdomains span across the interface on purpose. This approach is motivated by the error assessment of physics-based block preconditioners, revealing an accumulation of the error at the coupling surface, despite their overall efficiency.

5.2.2 Usage examples

Thermo-mechanical coupling In the following paragraph, a small overview of the literature is presented regarding the application of monolithic solvers to the thermo-mechanical coupled problem. Carter and Booker (1989) suggests a monolithic approach to the thermoelastic problem at small strains. The constitutive laws considered do not acknowledge the dependence of the mechanical properties on the temperature and are not deduced from a Helmholz energy function. Glaser (1992) uses monolithic algorithms for the calculation of thin-walled structures using shell elements and an arc-length method for the TSI solution. While all coupling terms were considered, only a simplified mechanical dissipation was included where the hardening power was neglected (according to Danowski (2014)). Ibrahimbegovic and Chorfi (2002) presents a thermoplasticity covariant formulation within the framework of the principal axis methodology, which the authors claim, leads to a very efficient numerical implementation. The paper contains several numerical simulations dealing with the fully coupled thermomechanical response at large viscoplastic strains, including strain localization and cyclic loading cases, to illustrate the performance of the proposed methodology. The authors consider the von Mises thermoplasticity yield criterion and strain energy depending on logarithmic stretches, a hardening variable, and temperature. A monolithic solver achieves the solution to the coupled problem, but no details about it are given. Danowski (2014) proposes a volume-coupled TSI model based on the finite element method for the structural and thermal field. Various temperature-dependent, isotropic, elastic, and elastoplastic material models for small and finite strains are employed, incorporating the effect of the highly elevated temperatures predominating in rocket nozzles, the practical application focused in the Ph.D. thesis. The author considers both monolithic and partitioned coupling algorithms to solve fully coupled thermomechanical systems. Regarding the former, a novel monolithic Newton-Krylov scheme with problem-specific block Gauss-Seidel preconditioner and algebraic multigrid methods is introduced. Concerning the latter, loosely and strongly coupled partitioned schemes are examined, possibly including acceleration techniques, as, e.g., the Aitken Δ^2 method. Netz (2013) and Rothe et al. (2015) both present monolithic approaches, based on the multilevel Newton method, for the solution of the thermo-mechanical problem. In both contributions, thermo-visco-plastic materials are successfully analyzed. Recently, Felder et al. (2021) have presented a finite strain thermo-mechanically coupled two-surface damage-plasticity theory. The authors obtain the solution for the three coupled fields, displacement, nonlocal damage variable, and temperature, employing an implicit and monolithic solution scheme.

The thermo-mechanical coupling has also been studied in the more specific domain of contact mechanics. Zavarise et al. (1992) present one of the earliest contributions in this direction. They propose a FEM formulation of frictionless contact, accounting for full thermo-elastic coupling. The penalty method is used to enforce the non-penetration conditions. Another contribution, Hansen (2011), advances a standard mortar discretization with Lagrange multipliers to solve the small strain thermo-elasticity problem. The authors consider the heat equation coupled to linear mechanics through a thermal expansion term in their formulation. The solution approach is based on a preconditioned Jacobian-free Newton Krylov solution method, and the use case under analysis is a light water reactor nuclear fuel rod. Dittmann et al. (2014) investigate thermomechanical mortar contact algorithms and their application to NURBS-based Isogeometric Analysis in the context of nonlinear

elasticity. Mortar methods are applied to both the mechanical and thermal fields to model frictional contact, the energy transfer between the surfaces, and frictional heating. A monolithic approach is pursued in solving the nonlinear algebraic equations found after the discretization in time and space. In the Ph.D. thesis by the same first author, Dittmann (2017), this approach is further pursued in multi-field contact problems. More recently, Seitz et al. (2018); Seitz (2019) tackles the numerical treatment of contact problems considering inelastic deformation and thermomechanical coupling. It accounts for plastic spin, visco-plasticity, and thermo-plastic coupling, as well as temperature-dependent material parameters. The authors also opt for a monolithic solver, although no further details are supplied. See also, in the context of contact mechanics, Oancea and Laursen (1997); Pantuso et al. (2000); Hüeber and Wohlmuth (2009); Hesch and Betsch (2011); Gitterle (2012) and Novascone et al. (2015).

Others In the context of fluid-structure interaction, the monolithic approach seems to be more widely used than in thermo-mechanically coupled problems. A few contributions in this domain using a monolith approach are Blom (1998); Heil (2004); Hübner et al. (2004); Michler et al. (2004); Zhang and Hisada (2004); Dettmer and Perić (2006); Hron and Turek (2006); Tezduyar et al. (2006); Küttler et al. (2010); Gee et al. (2011); Klöppel et al. (2011); Mayr et al. (2015) and Mayr et al. (2020). The use of a monolithic approach can also be found in the domain of saturated soils (e.g., Lewis and Sukirman (1993), Borja et al. (1998), Jha and Juanes (2007), White and Borja (2008)). Monolithic solvers are also used in the context of magnetohydrodynamics (e.g., Shadid et al. (2010) and Badia et al. (2014)).

5.3 Partitioned

The following Section presents the partitioned time-stepping algorithms. For a detailed comparison with the monolithic approach and between themselves, see Section **??**.

A field partition is a field-by-field decomposition of the space discretization. Partitioning may be algebraic or differential. In algebraic partitioning, the complete coupled system is spatially discretized first and then decomposed. In differential partitioning, the decomposition is done first, and each field is then discretized separately. Differential partitioning often leads to non-matched meshes, as typical of fluid-structure interaction. Algebraic partitioning was initially developed for matched meshes and substructuring (Felippa et al., 2001).

The earliest contributions regarding the partitioned treatment of coupled systems emerged the mid 1970s, involving structure-structure interactions and fluid-structure interactions (see e.g. Belytschko and Mullen (1976), Park et al. (1977), Belytschko and Mullen (1978), Hughes and Liu (1978) and Belytschko et al. (1979)).

Given a complex system, there are usually many ways of partitioning it into subsystems or fields. Felippa and Park (1980) provide a very pragmatic and helpful criterion to select the fields to be considered. According to their definition, a field is characterized by computational considerations. It is a segment of the overall problem for which a separable software module is either available or readily prepared if the interaction terms are suppressed. As such, a partitioned approach to the solution of multi-physics problems employs field analyzers specific to each field separately stepped in time. The coupling between the fields is achieved through proper

communication between the individual components using prediction, substitution, and synchronization techniques.

Before moving on, it may be helpful to clear up the difference between partitioned schemes, staggered schemes, operator splits, and fractional-step methods. The first is probably the most general term and includes the others. Its definition has already been given. A staggered scheme is a term most often used for the partitioned schemes where the solution concerning each field is sequential and obtained only once per time step as in the loosely coupled schemes to be introduced. However, it may also include the strongly coupled schemes, as well. An operator split is obtained through the decomposition of the fully coupled problem into subproblems. The structure of the problem is the same, as well as the unknowns considered. The only difference between the subproblems is the physical effects considered. The equation terms concerning each physical effect must be divided exclusively and exhaustively between the subproblems. Finally, according to Armero and Simo (1992) staggered algorithms for coupled problems can be viewed as fractional steps methods, in the sense of Holt and Yanenko (2012), arising from an operator split of the coupled problem of evolution.

5.3.1 Operator splits

The most common operator splits into thermomechanical problems are the isothermic and adiabatic split.

Isothermic The isothermic split is perhaps the most straightforward and natural approach, as noted by Argyris and Doltsinis (1981), one of the earliest contributions on the topic. The scheme achieves the solution of the thermo-mechanical problem, first solving the mechanical problem at a constant temperature, then a purely thermal phase is considered at a fixed configuration.

Adiabatic The adiabatic split is proposed in Armero and Simo (1992). It consists of a first phase where constant entropy is enforced and the second phase of purely thermal conduction at a fixed reference. In terms of implementation complexity, it is comparable to the isothermal split. This is possible because the constant entropy phase can be cast as a mechanical phase, where the stiffness and the external force are adjusted as a function of an intermediate temperature. This temperature is computed considering the strong form of the temperature evolution equation to retain the computational efficiency of the isothermal split, despite the momentum equation being enforced in its weak form. The advantage of this split is that when used in a staggered scheme, it is unconditionally stable (see Section **??**).

5.3.2 Loosely vs. Strongly coupled schemes

According to Felippa et al. (2001) there are several basic techniques associated with partitioned schemes (see Figure 5.1). These are

- preditction;
- substitution;
- interfield iteration;

- full step correction;
- lockstep advancing;
- midpoint correction;
- subcycling;
- augmentation.

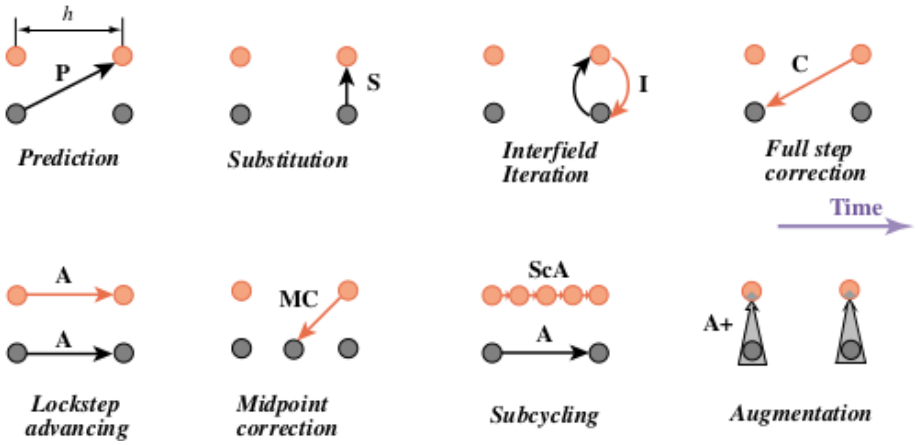

Figure 5.1: Devices of partitioned analysis time-stepping (Felippa et al., 2001).

Inter-field iterations are the primary criterion distinguishing loosely or one-way staggered coupled schemes and strongly or iterative staggered coupled schemes. In the loosely coupled schemes, the integration algorithm proceeds sequentially, solving the problem in each field only once per time step. On the other hand, for strongly coupled schemes, inter-field iterations are present, such that the problems are solved multiple times at the same time instant. This inner loop is repeated until a given tolerance is reached for the unknowns in each field.

The remainder of the techniques listed will be mentioned and explained in the discussion below.

5.3.3 Loosely coupled

The solution for the fully coupled problem is found in loosely coupled schemes by solving each field sequentially. For the thermomechanical problem, the two available schemes are the isothermal split (see e.g. Simo and Armero (1992), Agelet de Saracibar (1998)) and the adiabatic split (see e.g. Armero and Simo (1992) and Armero and Simo (1993)), as mentioned above.

According to Felippa et al. (2001), in linear problems, the first concern with partitioning is the degradation of time-stepping stability. After the analyst has ensured stability, an accuracy analysis of the method should be performed. In strongly nonlinear problems, such as fluid flow, stability and accuracy tend to be intertwined since numerical stability is harder to define. As such, they are usually considered together in method design. The expectation is for a method that operates well at a reasonable timestep.

Felippa and Geers (1988) presents a detailed explanation about how to design from scratch a loosely coupled time-stepping algorithm applicable to linear systems of equations. It includes implementation details, such as the choice of the predictor formula, and the design steps, from the formulation of the original field equations and temporal discretization to the stability and accuracy analysis. Other contributions focused mainly on linear systems are Neishlos (1983), Zienkiewicz et al. (1988) and Combescure and Gravouil (2002),

Because the loosely coupled schemes are explicit, they are also often only conditionally stable. The isothermic split is such an example (Armero and Simo, 1992). On the other hand, the adiabatic split proposed in Armero and Simo (1992) is unconditionally stable, despite being explicit. Farhat et al. (1991) also propose a stable staggered scheme, achieved through semi-algebraic augmentation, which, however, is limited to linearized thermoelasticity. In the context of coupled flow and geomechanics, Kim et al. (2011b) show that when the mechanical problem is solved first, the drained split combined with a backward Euler discretization is conditionally stable, and the undrained split is unconditionally stable when combined with midpoint rule. When instead the flow problem is solved, Kim et al. (2011a) show that the fixed-stress split is conditionally and the fixed-strain split is unconditionally stable for appropriate choices of the generalized midpoint rule.

Moreover, in the domain of fluid-structure interactions, it can be shown that staggered methods are inherently non-conservative. As time progresses in the simulation, these schemes introduce parasitic energy at the boundary, which contributes to their poor numerical stability (Michler et al., 2003). A further problem appears when solving these coupled physical problems, the so-called artificial added-mass effect, which manifests itself when a slender structure and fluid have similar densities, and the latter is modeled as an incompressible fluid leads to instability (Causin et al., 2005; Förster, 2007). It can even be shown that for every sequentially staggered scheme and spatial discretization of a problem, a mass ratio between the fluid and structural mass density can be found at which the coupled system becomes unstable (Förster et al., 2007).

Despite this, some contributions detail strategies allowing for the unconditional stability of these schemes. As part of the development loop of commercial tire designs, Gillard (2019) tackles the problem of tire hydroplaning. The author presents a robust explicit coupling scheme that relies on rigorous control of the energy artificially introduced at the interface by the staggering process through a dynamic adaptation of the coupling time step size. Regarding the artificial added-mass effect, Farhat et al. (2010) demonstrates that even for fluid-structure applications with strong added mass effects, a carefully designed staggered and sub-iteration-free time-integrator can achieve numerical stability and robustness concerning the slenderness of the structure, as long as the fluid is justifiably modeled as a compressible medium.

Another technique available to improve the stability of loosely coupled schemes is (algebraic) augmentation. It rests on the injection of one of the coupled equations into the other, after discretization in space, to 'soften' the system, either by reducing the large eigenvalues of the uncoupled stiff equation or by introducing some damping into it. Some examples of this approach include Park et al. (1977) and Park (1983).

Yet another technique to ensure stability in the context of fluid-structure interactions is presented in Fernández et al. (2006). Stability is achieved employing a semi-implicit coupling scheme, splitting the added-mass, viscous effects, and geometrical/convective nonlinearities, through a Chorin-Temam projection scheme

within the fluid.

Regarding accuracy, the loosely coupled schemes do not necessarily inherit the accuracy order of the schemes used in the integration of the separate fields, often being just of the first order in time (Farhat et al., 2006). However, some contributions detail approaches that are second-order time-accurate. In the context of thermo-elasticity, Armero and Simo (1992) show that a double-pass approach using the adiabatic split yields such a second-order accurate time-stepping algorithm. A few approaches yield similar results in the domain of fluid-structure interaction (see Piperno (1997), Farhat et al. (2006) and Farhat et al. (2010)). In any case, whatever the theoretical convergence order of the loosely coupled method, at a given time instant, the fully coupled discretized equations of the problem will never be exactly satisfied by the solutions found. There is a lag between the fields considered, e.g., the mechanical and thermal fields in a thermomechanical problem. In the context of strong coupling, this lag can be conceived as a numerical evaluation error. Solving approximately the exact (i.e., aggregated) equations can be reinterpreted as exactly solving a set of approximate (i.e., segregated) equations. Thus, one can construe loosely-coupled methods as solving a set of segregated equations instead of aggregated equations. Accordingly, the incurred numerical evaluation error can be reinterpreted as a discretization error. Loosely-coupled methods, therefore, satisfy conservation only in an asymptotic sense, i.e., for vanishing mesh width; this is a basic consistency requirement Michler (2005).

Prediction techniques can improve the order of the numerical evaluation error incurred by loosely-coupled partitioned methods. For the sake of explanation, consider the thermo-mechanical problem being solved using the isothermic split. When using predictors, instead of integrating the mechanical equations based on the structure's temperature in the previous time instant, a prediction can be used for the temperature of the structure boundary in the current time instant. Such predictions are generally based on an extrapolation of the solution from the previous time step. Prediction techniques improve the solution accuracy and stability of loosely-coupled methods (Piperno, 1997; Piperno and Farhat, 2001; Michler, 2005; Farhat et al., 2006).

Another technique available to improve the accuracy of the loosely coupled methods is subcycling. It involves solving each field's problems using different time steps since the fields present in a multi-physics problem often have different time scales. In the context of aeroelasticity, Piperno et al. (1995) claims that it can offer substantial computational advantages, including savings in the simulation CPU time because the structural field will be advanced fewer times. Farhat et al. (1997) and Piperno (1997) also argue for this technique along the same lines.

Usage examples The loosely coupled scheme has been used in the context of thermoelasticity (Argyris and Doltsinis, 1981; Armero and Simo, 1992; Johansson and Klarbring, 1993; Miehe, 1995a,b; Holzapfel and Simo, 1996), thermo-plasticity (Armero and Simo, 1992, 1993; Simo and Miehe, 1992; Wriggers et al., 1992; Agelet de Saracibar, 1998; Agelet de Saracibar et al., 1999) and thermo-viscoplasticity (Adam and Ponthot, 2002a,b).

For examples in aeroelasticity see e.g., Piperno et al. (1995); Farhat and Lesoinne (2000) and Farhat et al. (2003), and in fluid-structure interaction more broadly see e.g. Tezduyar et al. (2006) and Miller (2015) Other applications include fluid-soil interaction analysis (Saetta and Vitaliani, 1992; Armero, 1999; Mikelić and Wheeler, 2013).

5.3.4 Strongly coupled

In the strongly coupled scheme, inter-field iterations are performed until a given tolerance for the unknowns of each field is reached. They converge to the solution of the monolithic scheme and are thus able to satisfy discrete versions of the coupled problem exactly (Förster, 2007; Danowski, 2014). In principle, regarding thermomechanics, either the isothermal or the adiabatic slit can be used, but there seems to be no example of the latter. In contrast to the staggered schemes, there is no problem of conditional stability, but the scheme may converge very slowly or not at all. As an example coming from fluid-structure interactions, it has been shown that the number of coupling iterations increases when the time step decreases or when the structure becomes more flexible (Degroote et al., 2008). This can place a severe restriction on the use of these schemes. Several acceleration techniques are available in the literature to speed up convergence.

A straightforward way to improve the convergence behavior of the strongly coupled schemes is using predictors, in contrast to the values found in the last step. Thus, the initial guesses can be improved using well-chosen predictors Michler (2005). Along these lines, Erbts and Düster (2012) employs polynomial prediction methods, and Wendt et al. (2015) uses a line extrapolation method to improve the first guess of the unknown and thus decrease the number of iterations needed to achieve convergence.

Another approach that is well established for series acceleration is the Aitken delta-squared process. It uses previously computed values to obtain more accurate estimates for the unknown. Irons and Tuck (1969) is an early contribution detailing this low-memory convergence acceleration scheme. In the context of thermomechanics, Danowski (2014), Erbts et al. (2015) and Wendt et al. (2015) use this technique, with the last authors also employing a quasi-Newton least squares method. Some examples of contributions in the domain of fluid-structure interactions taking advantage of this approach are Degroote et al. (2008), Küttler and Wall (2008) and Küttler and Wall (2009). The last authors also introduce a vector extrapolation approach that includes more than three previous values of the iteration scheme in the improved estimate.

The strongly coupled approach lends itself to an interpretation as a nonlinear block Jacobi or Gauss-Seidel scheme, whose convergence is conditional and at most linear (Matthies and Steindorf, 2003b; Joosten et al., 2009). Cervera et al. (1996) provides an in-depth analysis of block Jacobi and Gauss-Seidel schemes applied to coupled problems, including considerations regarding efficiency, complexity, and parallelization. Matthies and Steindorf (2003a,b) suggests a block-Newton method instead, with the Jacobian of the system being approximate by a finite difference method. Under some assumptions on the subsystem solvers, this approach converges quadratically. Michler et al. (2005) propose a solution method based on the conjugation of sub-iterations via a Newton-Krylov method, which confines the GMRES acceleration to the interface degrees-of-freedom. The latter renders storage requirements for the Krylov space and computational cost of the least-squares problem low. The nesting of Newton and GMRES iterations lends itself to the reuse of Krylov vectors in subsequent linear system solutions. Küttler and Wall (2009) claims that the approach proposed by the last authors should not be regarded as a Newton-based solver but as a Krylov-based vector extrapolation scheme

One can also improve the convergence speed of the strongly coupled scheme using reduced-order models to produce a more accurate first guess and thus decrease the

number of iterations needed for the method to converge. Vierendeels et al. (2007) presents a technique that uses the Jacobian from reduced-order models that are built up during the coupling iterations. The reduced-order model is built for each step and approximates an arbitrary interface displacement fitting a linear regression to the previous displacement-stress points. Degroote et al. (2008) follows the same technique, coupling it with an Aitken delta-squared process.

Blom (2017) proposes a manifold mapping technique to decrease the number of sub-iterations of a high-fidelity fluid-structure interaction model. The idea is to perform many sub-iterations with a low-fidelity model instead of the high-fidelity flow and structure models.

Usage examples Regarding the use of strongly coupled schemes in the context of thermo-mechanics, there are a few contributions. Erbts and Düster (2012) present results concerning thermo-elasticity at finite strains, Netz (2013) concerning thermo-viscoelasticity, Danowski (2014) includes results on thermo-elasticity and thermo-elasto-plasticity. In field of fluid-structure interaction, a few examples of the use of strongly coupled schemes are Torii et al. (2006), Wall et al. (2007) and Blom (2017). Including more than two fields, Erbts et al. (2015) tackles electro-thermo-mechanical problems, as does Wendt et al. (2015), which also considers radiative heat transfer. In Lenarda and Paggi (2016), the strongly coupled scheme is used to solve coupled hygro-thermo-mechanical problems in photovoltaic laminates.

5.4 Comparison of solution techniques

According to Felippa and Geers (1988), the desirable properties of a time-stepping algorithm for solving coupled problems are:

- enjoys unconditional stability;
- is highly accurate;
- is easy to implement;
- is not memory intensive;
- requires low CPU time;
- satisfies software modularity constraints.

In the following, the time-stepping schemes presented above are compared with these criteria in mind. The application in view is thermomechanics.

Stability Regarding stability, the loosely coupled using an isothermal split is conditionally stable (Armero and Simo, 1992). Despite this, the limitation is not significant for metals plasticity, according to Simo and Miehe (1992). However, examples where the scheme diverges, can be found in Armero and Simo (1992). In this last contribution, the adiabatic split is introduced and shown to be unconditionally stable in the context of thermo-elasticity. Armero and Simo (1993) show that these properties extend to thermo-plasticity. The strongly coupled schemes are unconditionally stable because no critical time step leads to numerical instabilities in

the results. Despite this, the inner loop of the scheme may converge slowly or not at all Matthies and Steindorf (2003b). It depends on the spectral radius of the matrices involved (Cervera et al., 1996). There are, however, acceleration techniques that can mitigate this problem, including predictors and Aitken Δ^2 methods (see Section **??**). Danowski (2014) presents a numerical example concerning an internal pressurized thick-walled cylinder, whose material is viscoplastic, for which the strongly coupled scheme employed diverged, despite the use of an Aitken method. On the other hand, the monolithic scheme, as long as appropriately preconditioned, is unconditionally stable (Danowski, 2014).

Accuracy Regarding accuracy, the solution found from the loosely coupled method will never exactly satisfy the fully coupled discretized equations of the problem. There will be a time lag between the thermal and the mechanical field. Loosely-coupled methods, therefore, satisfy conservation only in an asymptotic sense, i.e., for vanishing mesh width (Michler, 2005). As long as it does not diverge, the monolithic and strongly coupled satisfy the coupled discretized equations exactly.

Ease of implementation The partitioned schemes are much easier to implement as most of them can work with the field analyzers as black boxes, concerning themselves only with communication between the solvers, initial guesses, and acceleration schemes using previously computed values. The monolithic scheme requires the computation of the full stiffness matrix, including the mixed terms and appropriate preconditioning that varies widely with the specific multi-physics problem to be solved.

Memory requirements When it comes to memory requirements, the partitioned schemes often require only the diagonal blocks of the stiffness matrix found in the linearization process. Previous values also need to be saved from one iteration to the next, increasing the memory cost for some acceleration techniques. In contrast, the fully coupled monolithic scheme requires the full stiffness matrix of the coupled problem.

CPU time According to Michler (2005), solving a fluid-structure interaction problem with the same accuracy using a loosely and strongly coupled scheme, the latter is more efficient than the former. For the same total number of iterations, the difference in the accuracy reached ranges from one to three orders of magnitude. These results run counter to a claim in Felippa et al. (2001). However, this is not supported by any numerical results from the last authors. In the numerical examples presented in Danowski (2014), the monolithic solver is in most cases faster than a strongly coupled scheme employing an Aitken method for problems in thermomechanics. The differences range from 120% to 140% in favor of the monolithic scheme. Supporting evidence for these conclusions can also be found in Novascone et al. (2015). The authors report CPU time ratios between the strongly coupled and monolithic approaches, ranging from 0.635 to 3.75 on the magnitude of the coupling.

Software modularity The partitioned approaches can take full advantage of software, including closed source commercial solvers. There is little to no software reuse for the monolithic approach, save for routines that solve linear systems and the like.

Conclusions Lastly, it may be helpful to reproduce the recommendations given in Felippa et al. (2001) regarding the choice between partitioned and monolithic approaches. According to the authors, the circumstances that favor the partitioned approach for tackling a coupled problem are a research environment with few delivery constraints, access to existing software, localized interaction effects (e.g., surface versus volume), and widespread spatial/temporal component characteristics. The opposite circumstances: commercial environment, rigid deliverable timetable, massive software development resources, global interaction effects, and comparable length/time scales favors a monolithic approach.

Putting it all together, the most appropriate choice for the present use case is the strongly coupled schemes with appropriate acceleration techniques. They can take advantage of already existing software, provide accurate results that agree with a monolithic approach, are not memory intensive, are easy to implement, and with the use of convergence acceleration techniques, are competitive from the computational efficiency standpoint. The only drawback seems to be the possibility of divergence in the inner loop, stalling the progress of the simulation.

Table 5.1: Summary of the comparison between the FFT-Galerkin method.

	Partitioned schemes		Monolithic
	Loosely coupled	Strongly coupled	
Stability	Isothermic split: conditionally stable Adiabatic split: unconditionally stable	unconditionally stable*	unconditionally stable
Accuracy	Coupled discretized equations not satisfied exactly	Coupled discretized equations satisfied	Coupled discretized equations satisfied
Ease of implementation	Only communication between field analyzers stricly needed		Full coupling needed: • Computation of mixed terms of the Jacobian • Preconditioning needed
Memory requirements	Only diagonal blocks of the full stiffness matrix needed		Full stiffness matrix needed
Software modularity constraints	Full software modularity		Poor or no software modularity

* The inner loop of the strongly coupled scheme may converge very slowly or even diverge.

Bibliography

Adam, L. and J.-P. Ponthot
2002a. Numerical simulation of viscoplastic and frictional heating during finite deformation of metal. Part I: Theory. *Journal of engineering mechanics*, 128(11):1215–1221. Publisher: American Society of Civil Engineers.

Adam, L. and J.-P. Ponthot
2002b. Numerical simulation of viscoplastic and frictional heating during finite deformation of metal. Part II: Applications. *Journal of engineering mechanics*, 128(11):1222–1232. Publisher: American Society of Civil Engineers.

Agelet de Saracibar, C.
1998. Numerical analysis of coupled thermomechanical frictional contact problems. Computational model and applications. *Archives of Computational Methods in Engineering*, 5(3):243–301.

Agelet de Saracibar, C., M. Cervera, and M. Chiumenti
1999. On the formulation of coupled thermoplastic problems with phase-change. *International Journal of Plasticity*, 15(1):1–34.

Argyris, J. H. and J. S. Doltsinis
1981. On the natural formulation and analysis of large deformation coupled thermomechanical problems. *Computer Methods in Applied Mechanics and Engineering*, 25(2):195–253.

Armero, F.
1999. Formulation and finite element implementation of a multiplicative model of coupled poro-plasticity at finite strains under fully saturated conditions. *Computer Methods in Applied Mechanics and Engineering*, 171:205–241.

Armero, F. and J. C. Simo
1992. A new unconditionally stable fractional step method for non-linear coupled thermomechanical problems. *International Journal for Numerical Methods in Engineering*, 35(4):737–766. _eprint: https://onlinelibrary.wiley.com/doi/pdf/10.1002/nme.1620350408.

Armero, F. and J. C. Simo
1993. A priori stability estimates and unconditionally stable product formula algorithms for nonlinear coupled thermoplasticity. *International Journal of Plasticity*, 9(6):749–782.

Badia, S., A. F. Martín, and R. Planas
2014. Block recursive LU preconditioners for the thermally coupled incompressible inductionless MHD problem. *Journal of Computational Physics*, 274:562–591.

Belytschko, T. and R. Mullen
1976. Mesh partitions of explicit-implicit time integration. *Formulations and computational algorithms in finite element analysis*, Pp. 673–690. Publisher: MIT Press: New York.

Belytschko, T. and R. Mullen
1978. Stability of explicit-implicit mesh partitions in time integration. *International Journal for Numerical Methods in Engineering*, 12(10):1575–1586. Publisher: Wiley Online Library.

Belytschko, T., H.-J. Yen, and R. Mullen
1979. Mixed methods for time integration. *Computer Methods in Applied Mechanics and Engineering*, 17:259–275. Publisher: Elsevier.

Blom, D.
2017. *Efficient numerical methods for partitioned fluid-structure interaction simulations*. Ph.D., Delft University of Technology, Netherlands.

Blom, F. J.
1998. A monolithical fluid-structure interaction algorithm applied to the piston problem. *Computer methods in applied mechanics and engineering*, 167(3-4):369–391. Publisher: Elsevier.

Borja, R., C. Tamagnini, and E. Alarćon
1998. Elastoplastic consolidation at finite strain part 2: finite element implementation and numerical examples. *Computer Methods in Applied Mechanics and Engineering*, 159:103–122.

Carter, J. P. and J. R. Booker
1989. Finite element analysis of coupled thermoelasticity. *Computers & Structures*, 31(1):73–80.

Causin, P., J.-F. Gerbeau, and F. Nobile
2005. Added-mass effect in the design of partitioned algorithms for fluid–structure problems. *Computer methods in applied mechanics and engineering*, 194(42-44):4506–4527. Publisher: Elsevier.

Cervera, M., R. Codina, and M. Galindo
1996. On the computational efficiency and implementation of block-iterative algorithms for nonlinear coupled problems. *Engineering Computations*, 13(6):4–30. Publisher: MCB UP Ltd.

Chen, K.
2005. *Matrix Preconditioning Techniques and Applications*, Cambridge Monographs on Applie. Cambridge University Press.

Combescure, A. and A. Gravouil
2002. A numerical scheme to couple subdomains with different time-steps for predominantly linear transient analysis. *Computer Methods in Applied Mechanics and Engineering*, 191(11):1129–1157.

Danowski, C.
2014. *Computational Modelling of Thermo-Structure Interaction with Application to Rocket Nozzles*. Ph.D., Technische Universität München, Germany.

Danowski, C., V. Gravemeier, L. Yoshihara, and W. A. Wall
2013. A monolithic computational approach to thermo-structure interaction. *International Journal for Numerical Methods in Engineering*, 95(13):1053–1078. _eprint: https://onlinelibrary.wiley.com/doi/pdf/10.1002/nme.4530.

Degroote, J., P. Bruggeman, R. Haelterman, and J. Vierendeels
2008. Stability of a coupling technique for partitioned solvers in FSI applications. *Computers & Structures*, 86(23):2224–2234.

Dettmer, W. and D. Perić
2006. A computational framework for fluid–structure interaction: Finite element formulation and applications. *Computer Methods in Applied Mechanics and Engineering*, 195(41):5754–5779.

Dittmann, M.
2017. *Isogeometric analysis and hierarchical refinement for multi-field contact problems*. Ph.D.

Dittmann, M., M. Franke, I. Temizer, and C. Hesch
2014. Isogeometric Analysis and thermomechanical Mortar contact problems. *Computer Methods in Applied Mechanics and Engineering*, 274:192–212.

Erbts, P. and A. Düster
2012. Accelerated staggered coupling schemes for problems of thermoelasticity at finite strains. *Computers & Mathematics with Applications*, 64(8):2408–2430.

Erbts, P., S. Hartmann, and A. Düster
2015. A partitioned solution approach for electro-thermo-mechanical problems. *Archive of Applied Mechanics*, 85(8):1075–1101.

Farhat, C., P. Geuzaine, and G. Brown
2003. Application of a three-field nonlinear fluid–structure formulation to the prediction of the aeroelastic parameters of an F-16 fighter. *Computers & Fluids*, 32:3–29.

Farhat, C. and M. Lesoinne
2000. Two efficient staggered algorithms for the serial and parallel solution of three-dimensional nonlinear transient aeroelastic problems. *Computer methods in applied mechanics and engineering*, 182(3-4):499–515. Publisher: Elsevier.

Farhat, C., M. Lesoinne, P. Stern, and S. Lanteri
1997. High performance solution of three-dimensional nonlinear aeroelastic problems via parallel partitioned algorithms: methodology and preliminary results. *Advances in Engineering Software*, 28:43–61.

Farhat, C., K. Park, and Y. Dubois-Pelerin
1991. An unconditionally stable staggered algorithm for transient finite element analysis of coupled thermoelastic problems. *Applied Mechanics and Engineering*, 85:349–365.

Farhat, C., A. Rallu, K. G. Wang, and T. Belytschko
2010. Robust and provably second-order explicit-explicit and implicit-explicit staggered time-integrators for highly non-linear compressible fluid-structure interaction problems. *International Journal for Numerical Methods in Engineering*, 84:73–107.

Farhat, C., K. Zee, and P. Geuzaine
2006. Provably second-order time-accurate loosely-coupled solution algorithms for transient nonlinear computational aeroelasticity. *Computer Methods in Applied Mechanics and Engineering*, 195:1973–2001.

Felder, S., N. Kopic-Osmanovic, H. Holthusen, T. Brepols, and S. Reese
2021. Thermo-mechanically coupled gradient-extended damage-plasticity modeling of metallic materials at finite strains. *International Journal of Plasticity*, P. 103142.

Felippa, C. and T. L. Geers
1988. Partitioned analysis for coupled mechanical systems. *Engineering Computations*, 5:123–133.

Felippa, C. A. and K. C. Park
1980. Staggered transient analysis procedures for coupled mechanical systems: Formulation. *Computer Methods in Applied Mechanics and Engineering*, 24(1):61–111.

Felippa, C. A., K. C. Park, and C. Farhat
2001. Partitioned analysis of coupled mechanical systems. *Computer Methods in Applied Mechanics and Engineering*, 190(24):3247–3270.

Fernández, M. A., J.-F. Gerbeau, and C. Grandmont
2006. A projection semi-implicit scheme for the coupling of an elasticstructure with an incompressible fluid. *International Journal for Numerical Methods in Engineering*.

Förster, C.
2007. Robust methods for fluid-structure interaction with stabilised finite elements.

Förster, C., W. A. Wall, and E. Ramm
2007. Artificial added mass instabilities in sequential staggered coupling of nonlinear structures and incompressible viscous flows. *Computer methods in applied mechanics and engineering*, 196(7):1278–1293. Publisher: Elsevier.

Gee, M. W., U. Küttler, and W. A. Wall
2011. Truly monolithic algebraic multigrid for fluid–structure interaction. *International Journal for Numerical Methods in Engineering*, 85(8):987–1016. _eprint: https://onlinelibrary.wiley.com/doi/pdf/10.1002/nme.3001.

Gillard, J.
2019. *An Efficient Partitioned Coupling Scheme for Tire Hydroplaning Analysis*. Ph.D., Technishcen Universität München, München.

Gitterle, M.
2012. *A dual mortar formulation for finite deformation frictional contact problems including wear and thermal coupling*. Ph.D., Technische Universität München.

Glaser, S.
1992. *Gekoppelte thermomechanische Berechnung duennwandiger Strukturen mit der Methode der Finiten Elemente.* Ph.D., Institute fuer Statik und Dynamik der Luft- und Raumfahrtkonstruktionen, University of Stuttgart.

Hansen, G.
2011. A Jacobian-free Newton Krylov method for mortar-discretized thermomechanical contact problems. *Journal of Computational Physics*, 230(17):6546–6562.

Heil, M.
2004. An efficient solver for the fully coupled solution of large-displacement fluid–structure interaction problems. *Computer Methods in Applied Mechanics and Engineering*, 193(1):1–23.

Hesch, C. and P. Betsch
2011. Energy-momentum consistent algorithms for dynamic thermomechanical problems—Application to mortar domain decomposition problems. *International Journal for Numerical Methods in Engineering*, 86(11):1277–1302. _eprint: https://onlinelibrary.wiley.com/doi/pdf/10.1002/nme.3095.

Holt, M. and N. Yanenko
2012. *The Method of Fractional Steps: The Solution of Problems of Mathematical Physics in Several Variables.* Springer Berlin Heidelberg.

Holzapfel, G. A. and J. C. Simo
1996. Entropy elasticity of isotropic rubber-like solids at finite strains. *Computer Methods in Applied Mechanics and Engineering*, 132(1):17–44.

Hron, J. and S. Turek
2006. A Monolithic FEM/Multigrid Solver for an ALE Formulation of Fluid-Structure Interaction with Applications in Biomechanics. In *Fluid-Structure Interaction.*, Lecture Notes in Computational Science and Engineering, vol 53.

Hughes, T. J. and W. Liu
1978. Implicit-explicit finite elements in transient analysis: stability theory.

Hübner, B., E. Walhorn, and D. Dinkler
2004. A monolithic approach to fluid–structure interaction using space–time finite elements. *Computer Methods in Applied Mechanics and Engineering*, 193(23):2087–2104.

Hüeber, S. and B. I. Wohlmuth
2009. Thermo-mechanical contact problems on non-matching meshes. *Computer Methods in Applied Mechanics and Engineering*, 198(15):1338–1350.

Ibrahimbegovic, A. and L. Chorfi
2002. Covariant principal axis formulation of associated coupled thermoplasticity at finite strains and its numerical implementation. *International Journal of Solids and Structures*, 39(2):499–528.

Irons, B. M. and R. C. Tuck
1969. A version of the Aitken accelerator for computer iteration. *International*

Journal for Numerical Methods in Engineering, 1(3):275–277. _eprint: https://onlinelibrary.wiley.com/doi/pdf/10.1002/nme.1620010306.

Jha, B. and R. Juanes
2007. A locally conservative finite element framework for the simulation of coupled flow and reservoir geomechanics. *Acta Geotechnica*, 2:139–153.

Johansson, L. and A. Klarbring
1993. Thermoelastic frictional contact problems: Modelling, finite element approximation and numerical realization. *Computer Methods in Applied Mechanics and Engineering*, 105(2):181–210.

Joosten, M. M., W. G. Dettmer, and D. Perić
2009. Analysis of the block Gauss–Seidel solution procedure for a strongly coupled model problem with reference to fluid–structure interaction. *International Journal for Numerical Methods in Engineering*, 78(7):757–778. _eprint: https://onlinelibrary.wiley.com/doi/pdf/10.1002/nme.2503.

Kim, J., H. Tchelepi, and R. Juanes
2011a. Stability and convergence of sequential methods for coupled flow and geomechanics: Drained and undrained splits. *Computer Methods in Applied Mechanics and Engineering*, 200:2094–2116.

Kim, J., H. Tchelepi, and R. Juanes
2011b. Stability and convergence of sequential methods for coupled flow and geomechanics: Fixed-stress and fixed-strain splits. *Computer Methods in Applied Mechanics and Engineering*, 200:1591–1606.

Klöppel, T., A. Popp, U. Küttler, and W. A. Wall
2011. Fluid–structure interaction for non-conforming interfaces based on a dual mortar formulation. *Computer Methods in Applied Mechanics and Engineering*, 200(45):3111–3126.

Küttler, U., M. Gee, C. Förster, A. Comerford, and W. A. Wall
2010. Coupling strategies for biomedical fluid–structure interaction problems. *International Journal for Numerical Methods in Biomedical Engineering*, 26(3-4):305–321. _eprint: https://onlinelibrary.wiley.com/doi/pdf/10.1002/cnm.1281.

Küttler, U. and W. A. Wall
2008. Fixed-point fluid–structure interaction solvers with dynamic relaxation. *Computational Mechanics*, 43(1):61–72.

Küttler, U. and W. A. Wall
2009. Vector Extrapolation for Strong Coupling Fluid-Structure Interaction Solvers. *Journal of Applied Mechanics*, 76(2).

Lenarda, P. and M. Paggi
2016. A geometrical multi-scale numerical method for coupled hygro-thermo-mechanical problems in photovoltaic laminates. *Computational Mechanics*, 57(6):947–963.

Lewis, R. and Y. Sukirman
1993. Finite element modelling of three-phase flow in deforming saturated

oil reservoirs. *International Journal for Numerical and Analytical Methods in Geomechanics*, 17(8):577–598. Publisher: Wiley Online Library.

Lin, P. T., J. N. Shadid, R. S. Tuminaro, M. Sala, G. L. Hennigan, and R. P. Pawlowski
2010. A parallel fully coupled algebraic multilevel preconditioner applied to multiphysics PDE applications: Drift-diffusion, flow/transport/reaction, resistive MHD. *International Journal for Numerical Methods in Fluids*, 64(10-12):1148–1179. tex.eprint: https://onlinelibrary.wiley.com/doi/pdf/10.1002/fld.2402.

Matthies, H. and J. Steindorf
2003a. Partitioned Strong Coupling Algorithms for Fluid-Structure-Interaction. *Computers & Structures*, 81:805–812.

Matthies, H. and J. Steindorf
2003b. Strong Coupling Methods.

Mayr, M., T. Klöppel, W. A. Wall, and M. W. Gee
2015. A Temporal Consistent Monolithic Approach to Fluid-Structure Interaction Enabling Single Field Predictors. *SIAM Journal on Scientific Computing*, 37(1):B30–B59. Publisher: Society for Industrial and Applied Mathematics.

Mayr, M., M. H. Noll, and M. W. Gee
2020. A hybrid interface preconditioner for monolithic fluid–structure interaction solvers. *Advanced Modeling and Simulation in Engineering Sciences*, 7(1):15.

Michler, C.
2005. *Efficient numerical methods for fluid-structure interaction*. Ph.D., Delft University of Technology, Netherlands. ISBN: 90-9019533-5.

Michler, C., E. H. v. Brummelen, S. J. Hulshoff, and R. d. Borst
2003. The relevance of conservation for stability and accuracy of numerical methods for fluid–structure interaction. *Computer Methods in Applied Mechanics and Engineering*, 192(37):4195–4215.

Michler, C., S. Hulshoff, E. Van Brummelen, and R. De Borst
2004. A monolithic approach to fluid–structure interaction. *Computers & fluids*, 33(5-6):839–848. Publisher: Elsevier.

Michler, C., E. H. van Brummelen, and R. de Borst
2005. An interface Newton–Krylov solver for fluid–structure interaction. *International Journal for Numerical Methods in Fluids*, 47(10-11):1189–1195. _eprint: https://onlinelibrary.wiley.com/doi/pdf/10.1002/fld.850.

Miehe, C.
1995a. Entropic thermoelasticity at finite strains. Aspects of the formulation and numerical implementation. *Computer Methods in Applied Mechanics and Engineering*, 120(3):243–269.

Miehe, C.
1995b. A theory of large-strain isotropic thermoplasticity based on metric transformation tensors. *Archive of Applied Mechanics*, 66(1):45–64.

Mikelić, A. and M. F. Wheeler
2013. Convergence of iterative coupling for coupled flow and geomechanics. *Computational Geosciences*, 17(3):455–461. Publisher: Springer.

Miller, B. A.
2015. *Loosely Coupled Time Integration of Fluid- Thermal-Structural Interactions in Hypersonic Flows*. Ph.D., Ohio State University.

Neishlos, H.
1983. Finite-Element Mesh Partitioning for Time Integration of Transient Problems. In *Numerical Solution of Partial Differential Equations: Theory, Tools and Case Studies: Summer Seminar Series Held at CSIR, Pretoria, February 8–10, 1982*, D. P. Laurie, ed., Pp. 225–245. Basel: Birkhäuser Basel.

Netz, T.
2013. *High-order space and time discretization scheme applied to problems of finite thermo-viscoelasticity*. Ph.D., Institute of Applied Mechanics, Clausthal University of Technology.

Novascone, S. R., B. W. Spencer, J. D. Hales, and R. L. Williamson
2015. Evaluation of coupling approaches for thermomechanical simulations. *Nuclear Engineering and Design*, 295:910–921.

Oancea, V. G. and T. A. Laursen
1997. A finite element formulation of thermomechanical rate-dependent frictional sliding. *International Journal for Numerical Methods in Engineering*, 40(23):4275–4311. _eprint: https://onlinelibrary.wiley.com/doi/pdf/10.1002/%28SICI%291097-0207%2819971215%2940%3A23%3C4275%3A%3AAID-NME257%3E3.0.CO%3B2-K.

Pantuso, D., K.-J. Bathe, and P. A. Bouzinov
2000. A finite element procedure for the analysis of thermo-mechanical solids in contact. *Computers & Structures*, 75(6):551–573.

Park, K.
1983. Stabilization of partitioned solution procedure for pore fluid-soil interaction analysis. *International Journal for Numerical Methods in Engineering*, 19:1669–1673.

Park, K., C. Felippa, and J. DeRuntz
1977. Stabilization of staggered solution procedures for fluid-structure interaction analysis. *Computational methods for fluid-structure interaction problems*, 26(94-124):51. Publisher: ASME New York.

Piperno, S.
1997. Explicit/implicit fluid/structure staggered procedures with a structural predictor and fluid subcycling for 2D inviscid aeroelastic simulations. *International Journal for Numerical Methods in Fluids*, 25:1207–1226.

Piperno, S. and C. Farhat
2001. Partitioned procedures for the transient solution of coupled aeroelastic problems–Part II: energy transfer analysis and three-dimensional applications. *Computer methods in applied mechanics and engineering*, 190(24-25):3147–3170. Publisher: Elsevier.

Piperno, S., C. Farhat, and B. Larrouturou
1995. Partitioned procedures for the transient solution of coupled aroelastic problems Part I: Model problem, theory and two-dimensional application. *Computer Methods in Applied Mechanics and Engineering*, 124:79–112.

Rothe, S., P. Erbts, A. Düster, and S. Hartmann
2015. Monolithic and partitioned coupling schemes for thermo-viscoplasticity. *Computer Methods in Applied Mechanics and Engineering*, 293:375–410.

Saetta, A. and R. Vitaliani
1992. Unconditionally convergent partitioned solution procedure for dynamic coupled mechanical systems. *International Journal for Numerical Methods in Engineering*, 33:1975–1996.

Seitz, A.
2019. *Computational Methods for Thermo-Elasto-Plastic Contact*. Ph.D., Technische Universität München, Germany.

Seitz, A., W. A. Wall, and A. Popp
2018. A computational approach for thermo-elasto-plastic frictional contact based on a monolithic formulation using non-smooth nonlinear complementarity functions. *Advanced Modeling and Simulation in Engineering Sciences*, 5(1):5.

Shadid, J., R. Pawlowski, J. Banks, L. Chacón, P. Lin, and R. Tuminaro
2010. Towards a scalable fully-implicit fully-coupled resistive MHD formulation with stabilized FE methods. *Journal of Computational Physics*, 229(20):7649–7671.

Simo, J. C. and F. Armero
1992. Recent Advances in the Numerical Analysis and Simulation of Thermoplasticity at Finite Strains.

Simo, J. C. and C. Miehe
1992. Associative coupled thermoplasticity at finite strains: Formulation, numerical analysis and implementation. *Computer Methods in Applied Mechanics and Engineering*, 98(1):41–104.

Smith, B., P. Bjorstad, and W. Gropp
2004. *Domain Decomposition: Parallel Multilevel Methods for Elliptic Partial Differential Equations*. Cambridge University Press.

Tezduyar, T. E., S. Sathe, R. Keedy, and K. Stein
2006. Space–time finite element techniques for computation of fluid–structure interactions. *Computer methods in applied mechanics and engineering*, 195(17-18):2002–2027. Publisher: Elsevier.

Torii, R., M. Oshima, T. Kobayashi, K. Takagi, and T. E. Tezduyar
2006. Computer modeling of cardiovascular fluid–structure interactions with the deforming-spatial-domain/stabilized space–time formulation. *Computer Methods in Applied Mechanics and Engineering*, 195(13-16):1885–1895. Publisher: Elsevier.

Verdugo, F. and W. A. Wall
2016. Unified computational framework for the efficient solution of n-field coupled problems with monolithic schemes. *Computer Methods in Applied Mechanics and Engineering*, 310:335–366.

Vierendeels, J., L. Lanoye, J. Degroote, and P. Verdonck
2007. Implicit coupling of partitioned fluid–structure interaction problems with reduced order models. *Computers & structures*, 85(11-14):970–976. Publisher: Elsevier.

Wall, W. A., S. Genkinger, and E. Ramm
2007. A strong coupling partitioned approach for fluid–structure interaction with free surfaces. *Computers & Fluids*, 36(1):169–183.

Wendt, G., P. Erbts, and A. Düster
2015. Partitioned coupling strategies for multi-physically coupled radiative heat transfer problems. *Journal of Computational Physics*, 300:327–351.

White, J. A. and R. Borja
2008. Stabilized low-order finite elements for coupled solid-deformation/fluid-diffusion and their application to fault zone transients. *Computer Methods in Applied Mechanics and Engineering*, 197:4353–4366.

Wriggers, P., C. Miehe, M. Kleiber, and J. C. Simo
1992. On the coupled thermomechanical treatment of necking problems via finite element methods. *International Journal for Numerical Methods in Engineering*, 33(4):869–883. _eprint: https://onlinelibrary.wiley.com/doi/pdf/10.1002/nme.1620330413.

Zavarise, G., P. Wriggers, E. Stein, and B. A. Schrefler
1992. Real contact mechanisms and finite element formulation—a coupled thermomechanical approach. *International Journal for Numerical Methods in Engineering*, 35(4):767–785. _eprint: https://onlinelibrary.wiley.com/doi/pdf/10.1002/nme.1620350409.

Zhang, Q. and T. Hisada
2004. Studies of the strong coupling and weak coupling methods in FSI analysis. *International Journal for Numerical Methods in Engineering*, 60(12):2013–2029. _eprint: https://onlinelibrary.wiley.com/doi/pdf/10.1002/nme.1034.

Zienkiewicz, O., D. K. Paul, and A. Chan
1988. Unconditionally stable staggered solution procedure for soil-pore fluid interaction problems. *International Journal for Numerical Methods in Engineering*, 26:1039–1055.